Geosci. Model Dev., 9, 2357–2376, 2016
www.geosci-model-dev.net/9/2357/2016/
doi:10.5194/gmd-9-2357-2016

Geoscientific Model Development
Open Access
EGU

Constraining the strength of the terrestrial CO_2 fertilization effect in the Canadian Earth system model version 4.2 (CanESM4.2)

Vivek K. Arora and John F. Scinocca

Canadian Centre for Climate Modelling and Analysis, Environment and Climate Change Canada, University of Victoria, Victoria, B.C., V8W 2Y2, Canada

Correspondence to: Vivek K. Arora (vivek.arora@ec.gc.ca)

Received: 17 November 2015 – Published in Geosci. Model Dev. Discuss.: 15 January 2016
Revised: 26 May 2016 – Accepted: 29 May 2016 – Published: 7 July 2016

Abstract. Earth system models (ESMs) explicitly simulate the interactions between the physical climate system components and biogeochemical cycles. Physical and biogeochemical aspects of ESMs are routinely compared against their observation-based counterparts to assess model performance and to evaluate how this performance is affected by ongoing model development. Here, we assess the performance of version 4.2 of the Canadian Earth system model against four land carbon-cycle-focused, observation-based determinants of the global carbon cycle and the historical global carbon budget over the 1850–2005 period. Our objective is to constrain the strength of the terrestrial CO_2 fertilization effect, which is known to be the most uncertain of all carbon-cycle feedbacks. The observation-based determinants include (1) globally averaged atmospheric CO_2 concentration, (2) cumulative atmosphere–land CO_2 flux, (3) atmosphere–land CO_2 flux for the decades of 1960s, 1970s, 1980s, 1990s, and 2000s, and (4) the amplitude of the globally averaged annual CO_2 cycle and its increase over the 1980 to 2005 period. The optimal simulation that satisfies constraints imposed by the first three determinants yields a net primary productivity (NPP) increase from $\sim 58\,\mathrm{Pg\,C\,year^{-1}}$ in 1850 to about $\sim 74\,\mathrm{Pg\,C\,year^{-1}}$ in 2005; an increase of $\sim 27\,\%$ over the 1850–2005 period. The simulated loss in the global soil carbon amount due to anthropogenic land use change (LUC) over the historical period is also broadly consistent with empirical estimates. Yet, it remains possible that these determinants of the global carbon cycle are insufficient to adequately constrain the historical carbon budget, and consequently the strength of terrestrial CO_2 fertilization effect as it is represented in the model, given the large uncertainty associated with LUC emissions over the historical period.

1 Introduction

The evolution of the atmospheric CO_2 concentration in response to anthropogenic fossil fuel CO_2 emissions is determined by the rate at which a fraction of these emissions is taken up by the land and ocean. Had the land and ocean not provided this "ecosystem service" since the start of the industrial era, and not removed about 50 % of CO_2 emissions from the atmosphere (Knorr, 2009), the present concentration of CO_2 in the atmosphere would have been around 500 ppm, compared to its current value of around 400 ppm. Over land, temperate and boreal forests as well as forests in the tropical region are known to be sinks of atmospheric carbon (Ciais et al., 2013; Gourdji et al., 2012; Schimel et al., 2015). The sink in the tropical forests is, however, countered by anthropogenic land use change emissions (Phillips and Lewis, 2014). Over ocean, the uptake of anthropogenic carbon is observed to be larger in the high latitudes than in the tropical and subtropical regions (Khatiwala et al., 2009). The manner in which the land and ocean will continue to provide this ecosystem service in the future is of both scientific and policy relevance.

Future projections of atmospheric CO_2 concentration, $[CO_2]$, in response to continued anthropogenic CO_2 emissions, or alternatively projections of CO_2 emissions compatible with a given future $[CO_2]$ pathway, are based primarily on comprehensive Earth system models (ESMs), which include interactive land and ocean carbon-cycle components (Jones et al., 2013). The land and ocean carbon-cycle components in ESMs respond both to increases in $[CO_2]$ as well as the associated changes in climate. These carbon components also respond to changes in climate associated with other forcings including changes in concentration of non-CO_2 greenhouse

gases and aerosols, to nitrogen deposition, and over land to anthropogenic land use change (LUC).

The response of land and ocean carbon-cycle components to changes in $[CO_2]$ and the associated change in climate is most simply characterized in the framework of the 140-year long 1 % per year increasing CO_2 (1pctCO2) experiment, in which $[CO_2]$ increases at a rate of 1 % per year from pre-industrial value of about 285 ppm until concentration quadruples to about 1140 ppm. The 1pctCO2 experiment has been recognized as a standard experiment by the coupled model intercomparison project (CMIP), which serves to quantify the response of several climate and Earth system metrics to increasing CO_2. These metrics include the transient climate response (TCR) and the transient climate response to cumulative emissions (TCRE; Gillett et al., 2013). Arora et al. (2013) analysed results from fully , biogeochemically and radiatively coupled versions of the 1pctCO2 experiment from eight ESMs that participated in the phase five of the CMIP (CMIP5). They calculated the response of land and ocean carbon-cycle components to changes in $[CO_2]$ and the associated change in climate expressed in terms of carbon-concentration and carbon–climate feedbacks, respectively. Arora et al. (2013) found that of all the carbon-cycle feedbacks, the carbon-concentration feedback over land, which is primarily determined by the strength of the terrestrial CO_2 fertilization effect, is the most uncertain across models. They found that while the uncertainty in the carbon-concentration feedback over land (expressed in terms of the standard deviation of the magnitude of the feedbacks) had somewhat reduced since the first coupled carbon-cycle climate model intercomparison project (C^4MIP) (Friedlingstein et al., 2006), its uncertainty remained the largest of all carbon-cycle feedbacks. The comparison of the actual magnitudes of the carbon-cycle feedbacks over land is, however, not straightforward between the Arora et al. (2013) and Friedlingstein et al. (2006) studies because they used different CO_2 scenarios.

The reason for this large uncertainty is that it is fairly difficult at present to constrain the strength of the terrestrial CO_2 fertilization effect at the global scale. The net atmosphere–land CO_2 flux since the start of the industrial era has not only been influenced by the changes in $[CO_2]$ but also the associated change in climate (due both to changes in $[CO_2]$ and other climate forcers), nitrogen deposition, and more importantly land use change – the contribution of which itself remains highly uncertain. Since it is difficult to estimate the observed magnitude of net atmosphere–land CO_2 flux since the start of the industrial era, attributable only to the increase in $[CO_2]$, it is consequently difficult to estimate the strength of the terrestrial CO_2 fertilization effect.

Measurements at Free-Air CO_2 Enrichment (FACE) sites in which vegetation is exposed to elevated levels of $[CO_2]$ help to assess some aspects of CO_2 fertilization and how nutrients constraints regulate photosynthesis at elevated $[CO_2]$ (Medlyn et al., 1999; McGuire et al., 1995). However, FACE results cannot be easily extrapolated to the global scale and the response of vegetation corresponds to a step increase in $[CO_2]$ not the gradual increase, which the real-world vegetation is experiencing.

As part of the ongoing evaluation of carbon cycle in ESMs, the model simulated aspects of the global carbon cycle are routinely evaluated against their observation-based counterparts. These evaluations also provide the opportunity to adjust physical processes that influence the strength of the terrestrial CO_2 fertilization effect to provide the best comparison with observation-based aspects of the global carbon cycle. Here, we present results from such an evaluation for a new version of the Canadian Earth system model (CanESM4.2). An earlier version of the Canadian Earth system model (CanESM2; Arora et al., 2011) participated in the CMIP5 (Taylor et al., 2012) and its results also contributed to the fifth assessment report (AR5) of the Intergovernmental Panel on Climate Change (IPCC). We evaluate the response of CanESM4.2, for three different strengths of the terrestrial CO_2 fertilization effect, against four observation-based determinants of the global carbon cycle and the historical global carbon budget over the 1850–2005 period, with a focus on the land carbon-cycle component. These determinants include (1) globally averaged atmospheric CO_2 concentration, (2) cumulative atmosphere–land CO_2 flux, (3) atmosphere–land CO_2 flux for the decades of 1960s, 1970s, 1980s, 1990s, and 2000s, and (4) the amplitude of the globally averaged annual CO_2 cycle and its increase over the 1980 to 2005 period.

The strength of the CO_2 fertilization effect influences all four of these determinants of the global carbon cycle and the historical carbon budget. A stronger CO_2 fertilization effect, of course, implies a larger carbon uptake by land and consequently a lower rate of increase of $[CO_2]$ in response to anthropogenic fossil fuel emissions. However, the strength of the CO_2 fertilization effect also influences the amplitude of the annual $[CO_2]$ cycle, which is primarily controlled by the Northern Hemisphere's biospheric activity. The amplitude of the annual $[CO_2]$ cycle has been observed to increase over the past 5 decades, suggesting a gradual increase in photosynthesis in association with a strengthening of the CO_2 fertilization effect (Keeling et al., 1996; Randerson et al., 1997) and thus possibly can help to constrain the strength of the terrestrial CO_2 fertilization effect in Earth system models.

2 The coupled climate-carbon system and CanESM4.2

2.1 The coupled climate-carbon system

The globally averaged and vertically integrated carbon budget for the combined atmosphere–land–ocean system may be written as

$$\frac{\mathrm{d}H_\mathrm{G}}{\mathrm{d}t} = \frac{\mathrm{d}H_\mathrm{A}}{\mathrm{d}t} + \frac{\mathrm{d}H_\mathrm{L}}{\mathrm{d}t} + \frac{\mathrm{d}H_\mathrm{O}}{\mathrm{d}t} = E_\mathrm{F}, \quad (1)$$

where the global carbon pool $H_\mathrm{G} = H_\mathrm{A} + H_\mathrm{L} + H_\mathrm{O}$ is the sum of carbon in the atmosphere, land, and ocean components,

respectively (Pg C), and E_F is the rate of anthropogenic CO_2 emissions (Pg C year^{-1}) into the atmosphere. The equations for the atmosphere, land, and ocean components are written as

$$\begin{aligned}\frac{dH_A}{dt} &= F_A + E_F \\ &= -F_L - F_O + E_F \\ &= -(F_l - E_L) - F_O + E_F \\ &= -F_l - F_O + E_F + E_L \\ \frac{dH_L}{dt} &= F_L = F_l - E_L \\ \frac{dH_O}{dt} &= F_O, \end{aligned} \quad (2)$$

where $(F_L + F_O) = -F_A$ are the fluxes (Pg C year^{-1}) between the atmosphere and the underlying land and ocean, taken to be positive into the components. The net atmosphere–land CO_2 flux $F_L = F_l - E_L$ is composed of LUC emission rate E_L (Pg C year^{-1}) as well as the remaining global "natural" CO_2 flux F_l that is often referred to as the residual or missing land sink in the context of the historical carbon budget (Le Quéré et al., 2015). The emissions associated with LUC occur when natural vegetation, for example, is deforested and replaced by croplands resulting in net loss of carbon from land to the atmosphere (i.e. positive E_L). Conversely, when croplands are abandoned and gradually replaced by forests then carbon is gained from atmosphere into the land (i.e. negative E_L).

Over land, the rate of change of carbon is reflected in the model's three land pools (vegetation, V; soil, S; and litter or detritus, D)

$$\begin{aligned}\frac{dH_L}{dt} &= F_L = F_l - E_L \\ &= \frac{dH_V}{dt} + \frac{dH_S}{dt} + \frac{dH_D}{dt} \\ &= (G - R_A) - R_H - E_L \\ &= N - R_H - E_L, \end{aligned} \quad (3)$$

where G is the gross primary productivity (Pg C year^{-1}), which represents the rate of carbon uptake by vegetation through photosynthesis, and R_A and R_H are the autotrophic and heterotrophic respiratory fluxes (Pg C year^{-1}) from living vegetation and dead litter and soil carbon pools, respectively. $N = G - R_A$ is the net primary productivity (NPP), which represents the carbon uptake by vegetation after autotrophic respiratory costs have been taken into account. The heterotrophic respiration $R_H = R_{H,D} + R_{H,S}$ is composed of respiration from the litter and soil carbon pools. The rate of change in carbon in model's litter (H_D) and soil (H_S) pools is written as

$$\begin{aligned}\frac{dH_D}{dt} &= D_L + D_S + D_R - C_{D\to S} - R_{H,D} \\ \frac{dH_S}{dt} &= C_{D\to S} - R_{H,S}, \end{aligned} \quad (4)$$

where $D_{i,i=L,S,R}$ is the litter fall from the model's leaf, stem and root components into the model's litter pool. $C_{D\to S}$ is the transfer of humidified litter into the soil carbon pool calculated as a fraction of the litter respiration ($R_{H,D}$)

$$C_{D\to S} = \chi R_{H,D} \quad (5)$$

and χ is the humification factor.

Integrating Eqs. (2) and (3) in time with $\int_{t_0}^{t}(dH/dt)dt = H(t) - H(t_0) = \Delta H(t)$ and $\int_{t_0}^{t} F\,dt = \widetilde{F}(t)$ (Pg C) gives

$$\begin{aligned}\Delta H_A &= -\left(\widetilde{F}_O + \widetilde{F}_l\right) + \left(\widetilde{E}_F + \widetilde{E}_L\right) \\ \Delta H_O &= \widetilde{F}_O \\ \Delta H_L &= \widetilde{F}_L = \widetilde{F}_l - \widetilde{E}_L; \\ &= \Delta H_V + \Delta H_S + \Delta H_D = \widetilde{F}_l - \widetilde{E}_L = \widetilde{N} - \widetilde{R}_H - \widetilde{E}_L \\ \Delta H_l &= \widetilde{F}_l \\ \Delta H &= \widetilde{E}_F. \end{aligned} \quad (6)$$

The cumulative change in the atmosphere, the ocean and the land carbon pools is written as

$$\begin{aligned}\Delta H_A + \Delta H_O + \left(\Delta H_l - \widetilde{E}_L\right) &= \widetilde{E}_F \\ \Delta H_A + \Delta H_O + \Delta H_l &= \widetilde{E}_F + \widetilde{E}_L = \widetilde{E}, \end{aligned} \quad (7)$$

where $\widetilde{E}$ (Pg C) is the cumulative sum of the anthropogenic emissions from fossil fuel consumption and land use change. When emissions associated with LUC are zero, Eq. (7) becomes

$$\Delta H_A + \Delta H_O + \Delta H_L = \widetilde{E}_F = \widetilde{E}, \quad (8)$$

which indicates how cumulative emissions are parsed into changes in atmospheric carbon burden and carbon uptake by the ocean and land components.

2.2 Canadian Earth system model version 4.2

2.2.1 Physical components

At the Canadian Centre for Climate Modelling and Analysis (CCCma), the Earth system model, CanESM2, has undergone further development since its use for CMIP5. This version of the model has been equivalently labelled CanESM4.0 in an effort to rationalize the ESM naming convention to better reflect the fact that this model version employs the fourth generation atmosphere component, CanAM4, (Von Salzen et al., 2013) and the fourth generation ocean component,

CanOM4 (Arora et al., 2011). The version of the CCCma Earth system model used for this study is CanESM4.2 and therefore represents two full cycles of model development on all of its components. Similar to CanESM2, the physical ocean component of CanESM4.2 (CanOM4.2) has 40 levels with approximately 10 m resolution in the upper ocean while the horizontal ocean resolution is approximately 1.41° (longitude) × 0.94° (latitude). The majority of development in CanESM4.2, relative to CanESM2, has occurred on its atmospheric component CanAM4.2. CanAM4.2 is a spectral model employing T63 triangular truncation with physical tendencies calculated on a 128×64 ($\sim 2.81°$) horizontal linear grid with 49 layers in the vertical, whose thicknesses increase monotonically with height to 1 hPa. Relative to CanAM4, CanAM4.2 includes a new version of the Canadian Land Surface Scheme, CLASS3.6, which models the energy and water fluxes at the atmosphere–land boundary by tracking energy and water through the soil, snow, and vegetation canopy components (Verseghy, 2012). CLASS models the land surface energy and water balance and calculates liquid and frozen soil moisture, and soil temperature for three soil layers (with thicknesses 0.1, 0.25 and 3.75 m). The thickness of the third layer depends on the depth to bedrock (and is in many places less than 3.75 m) based on the Zobler (1986) soil data set. Changes to CLASS primarily include improvements to the simulation of snow at the land surface. These incorporate new formulations for vegetation interception of snow (Bartlett et al., 2006), for unloading of snow from vegetation (Hedstrom and Pomeroy, 1998), for the albedo of snow-covered canopies (Bartlett and Verseghy, 2015), for limiting snow density as a function of depth (Tabler et al., 1990; Brown et al., 2006), and for the thermal conductivity of snow (Sturm et al., 1997). Water retention in snowpacks has also been incorporated. CanAM4.2 also includes an aerosol microphysics scheme (von Salzen, 2006; Ma et al., 2008; Peng et al., 2012), a higher vertical resolution in the upper troposphere, a reduced solar constant ($1361\,W\,m^{-2}$) and an improved treatment of the solar continuum used in the radiative transfer. CanAM4.2 also considers natural and anthropogenic aerosols and their emissions, transport, gas-phase and aqueous-phase chemistry, and dry and wet deposition as summarized in Namazi et al. (2015)

2.2.2 Land and ocean carbon-cycle components

The ocean and land carbon-cycle components of CanESM4.2, are similar to CanESM2, and represented by the Canadian Model of Ocean Carbon (CMOC) (Christian et al., 2010) and the Canadian Terrestrial Ecosystem Model (CTEM) (Arora et al., 2009; Arora and Boer, 2010), respectively.

LUC emissions in CTEM are modelled interactively on the basis of changes in land cover, which are determined by changes in crop area. The historical land cover used in the simulations presented here is reconstructed using the linear approach of Arora and Boer (2010) and is the same as that used for CMIP5 simulations; as the fraction of crop area in a grid cell changes, the fraction of non-crop plant functional types (PFTs) is adjusted linearly in proportion to their existing coverage. The historical changes in crop area are based on the data set provided for CMIP5 simulations as explained in Arora and Boer (2014). When the fraction of crop area in a grid cell increases then the fractional coverage of other PFTs is reduced, which results in deforested biomass. The deforested biomass is allocated to three components that are (i) burnt instantaneously and contribute to (ii) short-term (paper) and (iii) long-term (wood products) pools (Arora and Boer, 2010). The deforested biomass corresponding to paper and wood products is transferred to model's litter and soil carbon pools, respectively. When the fraction of crop area decreases, the fractional coverage of non-crop PFTs increases and their vegetation biomass is spread over a larger area reducing vegetation density. Carbon is sequestered until a new equilibrium is reached providing a carbon sink associated with regrowth as the abandoned areas revert back to natural vegetation.

The LUC emissions term (E_L) in the Eqs. (1) through (8) is not easily defined or calculated. Pongratz et al. (2014) discuss the multiple definitions and methods of calculating E_L. When E_L is calculated using models, it is most usually defined as the difference in F_L between simulations with and without LUC. This is also the basic definition used by Pongratz et al. (2014). Calculating E_L thus requires performing additional simulations without land use change in which land cover is held constant at its pre-industrial state. For a simulation without LUC, Eq. (3) becomes

$$\frac{dH'_L}{dt} = F'_L = F'_I \tag{9}$$

and an estimate of E_L, and its cumulative values $\widetilde{E}_L$, is obtained as

$$\begin{aligned} E_L &= F'_L - F_L \\ \widetilde{E}_L &= \widetilde{F}'_L - \widetilde{F}_L. \end{aligned} \tag{10}$$

Over the historical period, globally, F'_L is expected to be higher than F_L (both considered positive downwards) due, at least, to two processes: (1) fraction of deforested biomass that is burnt and which contributes to short- and long-term product pools all release carbon to the atmosphere, albeit at different timescales, (2) the area that is deforested and put under agricultural use loses soil carbon and cannot sequester carbon in response to increase [CO_2] since crops are frequently harvested. As a result E_L is positive.

Relative to CanESM2, the version of CTEM employed in CanESM4.2, CTEM4.2, includes changes to the humification factor (χ; see Eqs. 4 and 5), which determines what fraction of the humidified litter is transferred from litter (H_D) to the soil carbon pool (H_S). The value of χ employed in CTEM4.2 has been changed for crop PFTs from 0.45 to 0.10,

which decreases the transfer of the humidified litter to the soil carbon pool. As a result, a decrease in global soil carbon over the historical period is obtained as natural vegetation is replaced by croplands as is seen in empirical measurements (Wei et al., 2014). This change in humification factor was required despite the higher litter decomposition rates over croplands and is discussed in more detail later in the results section. In addition, in CTEM4.2 the sensitivity of photosynthesis to soil moisture is reduced for coupling to CLASS 3.6, especially for the broadleaf evergreen PFT (which exists mainly in the tropics) to somewhat account for deep roots, for example in the Amazonian region (e.g. see da Rocha et al., 2004).

CTEM has always included a parameterization of photosynthesis down-regulation, which represents acclimatization to elevated CO_2 in the form of a decline in maximum photosynthetic rate. In the absence of explicit coupling of terrestrial carbon and nitrogen cycles this parameterization yields a mechanism to reduce photosynthesis rates as $[CO_2]$ increases. The photosynthesis down-regulation parameterization is described in detail in Arora et al. (2009) and is based on earlier simpler models, which expressed net or gross primary productivity (NPP or GPP) as a logarithmic function of atmospheric CO_2 concentration (e.g. Cao et al., 2001; Alexandrov and Oikawa, 2002).

$$G(t) = G_0\left(1 + \gamma_p \ln\left(\frac{C(t)}{C_0}\right)\right), \tag{11}$$

where GPP at any given time, $G(t)$, is a function of its initial value G_0, atmospheric CO_2 concentration at time t, $C(t)$, and its initial value C_0. The rate of increase of GPP is determined by the parameter γ_p (where p indicates the "potential" rate of increase of GPP with CO_2). The ratio of GPP in two different versions of a model in which GPP increases at different rates (γ_p and γ_d) is given by

$$\xi(C) = \frac{1 + \gamma_d \ln(C/C_0)}{1 + \gamma_p \ln(C/C_0)}, \tag{12}$$

where t is omitted for clarity. When $\gamma_d < \gamma_p$, the modelled potential gross photosynthesis rate (G_p), which is not constrained by nutrient limitation, can be multiplied by the scalar $\xi(C)$ (Eq. 12), which yields the gross primary productivity (G) used in Eq. (3) that now increases in response to CO_2 increases at a rate determined by the value of γ_d (the subscript d indicates down-regulation).

$$G = \xi(C) G_p. \tag{13}$$

A lower value of γ_d than γ_p yields a value of $\xi(C)$ that is less than one. As the concentration of CO_2, expressed as C in Eq. (12), increases above its pre-industrial level C_0 (285 ppm), $\xi(C)$ progressively decreases resulting in a gross primary productivity G, which is less than its potential value G_p. Figure 1 shows the behaviour of $\xi(C)$ for $\gamma_p = 0.95$

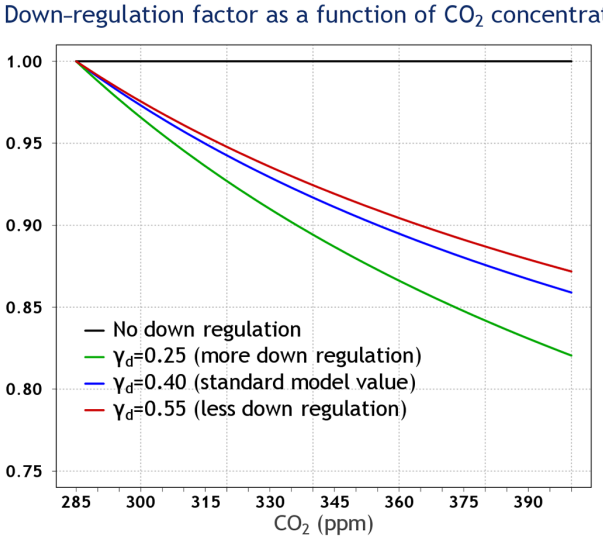

Figure 1. The behaviour of terrestrial photosynthesis down-regulation scalar $\xi(C)$ (Eq. 12) for $\gamma_p = 0.95$ and values of γ_d equal to 0.25, 0.4 and 0.55 that are used in CanESM4.2 simulations.

and three values of γ_d (0.25, 0.4, and 0.55) corresponding to three different strengths of the terrestrial CO_2 fertilization effect. A value of $\gamma_d = 0.25$ was used for CanESM2 to best simulate the globally averaged surface CO_2 concentration and cumulative 1850–2005 atmosphere–land CO_2 flux. CanESM2, however, was not as rigourously evaluated as we have attempted here for CanESM4.2. Through the parameter γ_d, the physical process of down-regulation has a direct influence on the strength of the terrestrial CO_2 fertilization effect. In practice, different combinations of γ_d and γ_p are able to yield very similar values of $\xi(C)$. Arora et al. (2009) calculated the value of γ_d based on results from six studies, two of which were meta-analyses each based on 15 and 77 individual studies, which grow plants in ambient and elevated CO_2 environments. Their results are equivalent to $\gamma_d = 0.46$ with a range from 0.22 to 0.63 for $\gamma_p = 0.95$.

In Fig. 1, while $\xi(C)$ decreases with an increase in atmospheric CO_2, indicating progressive decline in photosynthesis due to nutrient limitation, the slope $\frac{d\xi}{dC}$ also decreases. Although a second-order effect, this is a limitation of the current formulation of $\xi(C)$. A decreasing $\xi(C)$ as CO_2 increases can eventually also lead to a decrease in GPP although we have not seen this behaviour up to CO_2 concentration of around 1000 ppm in simulations performed with CanESM2 (see Arora and Boer, 2014). Whereas γ_d is used to model down-regulation of photosynthesis it may also be used as a measure of the strength of the CO_2 fertilization effect. Lower values of γ_d indicate higher down-regulation (see Fig. 1) so higher values of γ_d imply higher strength of the CO_2 fertilization effect. Finally, γ_d is specific to CTEM and as such the value of this parameter is irrelevant to other models. More relevant for comparison with other models is the simulated

rate of increase of NPP over the historical period that a given value of γ_d yields.

2.2.3 Treatment of CO_2 in the atmosphere

The land and ocean components of the carbon cycle in CanESM4.2 are operable for two experimental designs – (1) an emissions-driven mode, where the atmospheric CO_2 concentration is a freely evolving three-dimensional (3-D) tracer in the model and (2) a concentration-driven mode, where the atmospheric CO_2 concentration is prescribed externally.

In the emissions-driven mode the anthropogenic CO_2 emissions (E_F) are specified and since the interactive land and ocean carbon-cycle components simulate the F_L and F_O terms, respectively, the model is able to simulate the evolution of $[CO_2]$ through the H_A term, which represents the atmospheric carbon burden, in Eq. (2). This is referred to as the interactively simulated $[CO_2]$, or "free-CO2" configuration. In this case, the model simulates the transport of CO_2 in the atmosphere producing 3-D structure, an annual cycle, and inter-annual variability.

In the concentration-driven mode, the land and ocean CO_2 fluxes, F_L and F_O, remain interactively determined so model results can be used to diagnose the E_F term (based on Eq. 2) that is compatible with a given $[CO_2]$ pathway at the global scale. The concentration-driven mode can be executed in two CanESM4.2 configurations. In the first configuration, a single scalar value of $[CO_2]$, which may be time evolving, is imposed at all geographical and vertical locations in the model. This follows the CMIP5 prescription for concentration-driven simulations and we refer to it here as "specified-CO2" concentration-driven mode. In the second configuration, a new approach for specifying CO_2 concentration has been implemented in CanESM4.2. In this new approach, only the globally averaged concentration of CO_2 in the lowest model level is constrained by the prescribed value. The geographical and vertical distribution of CO_2 in the atmosphere and its annual cycle in this second configuration is otherwise free to evolve in the same manner as in the emissions-driven, free-CO2, configuration. A relaxation timescale of 1 day is employed in this new configuration and a fixed annual cycle, derived from the free-CO2 pre-industrial control simulation, is imposed on the reference value of $[CO_2]$. The reference value of $[CO_2]$ may additionally be specified as time evolving. We refer to this configuration as the "relaxed-CO2" concentration-driven mode. Aside from the relaxational constraint on the global-mean surface value of $[CO_2]$, the atmospheric configuration for relaxed-CO2 is identical to that for free-CO2 with zero emissions. As a consequence, the relaxed-CO2 configuration allows for the same non-linearlity in the atmosphere–surface exchange of CO_2 as the free-CO2 configuration leading to nearly identical spatial distribution and seasonal cycle of atmosphere CO_2 concentrations. In this regard, the relaxed-CO2 configuration is physically more realistic than the specified-CO2 configuration.

There are practical advantages to using the relaxed-CO2 configuration over the specified-CO2 configuration for concentration-driven simulations. When spinning up land and ocean carbon pools in a pre-industrial control simulation, the model is executed in concentration-driven mode to bring these pools into equilibrium with a prescribed CO_2 concentration. In earlier versions of the CanESM, a specified-CO2 configuration was used for this purpose. Beginning with version 4.1, the relaxed-CO2 configuration is used for this purpose because it produces little or no drift when used to initialize the free-CO2 pre-industrial control simulations. In fact, a relaxed-CO2 pre-industrial control simulation may be used as the control simulation for both emissions-driven and (relaxed-CO2) concentration-driven experiments. This is not the case when the specified-CO2 is used as the configuration for concentration-driven experiments.

3 Experimental set-up

Three different kinds of experiments are performed for this study. The first is the standard 1 % per year increasing CO_2 experiment (1pctCO2) performed for three different strengths of the terrestrial CO_2 fertilization effect. The 1pctCO2 is a concentration-driven experiment and we use the relaxed-CO2 configuration to specify CO_2 in the atmosphere. The second experiment is the CMIP5 1850–2005 historical experiment, referred to as "esmhistorical" following CMIP5 terminology, which is performed with specified anthropogenic CO_2 emissions (i.e. in emissions-driven, or free-CO2, mode), where $[CO_2]$ is simulated interactively. Concentrations of non-CO_2 greenhouse gases and emissions of aerosols and their precursors are specified in the esmhistorical experiment following the CMIP5 protocol. The third experiment is same as the esmhistorical experiment but LUC is not permitted and the land cover remains at its 1850 value; referred to as the esmhistorical_noluc experiment. Two ensemble members are performed for each of the three versions of the esmhistorical and esmhistorical_noluc experiments corresponding to three different strengths of the terrestrial CO_2 fertilization effect. The rationale for performing historical simulations without LUC is to be able to quantify LUC emissions E_L using Eq. (10). Table 1 summarizes all the simulations performed.

The 1pctCO2 simulations with relaxed CO_2 for three different strengths of the terrestrial CO_2 fertilization effect are initialized from a corresponding pre-industrial control simulation with CO_2 specified at ~ 285 ppm and all other forcings at their 1850 values. The esmhistorical and esmhistorical_noluc simulations are initialized from a pre-industrial control simulation with free CO_2 and zero anthropogenic CO_2 emissions.

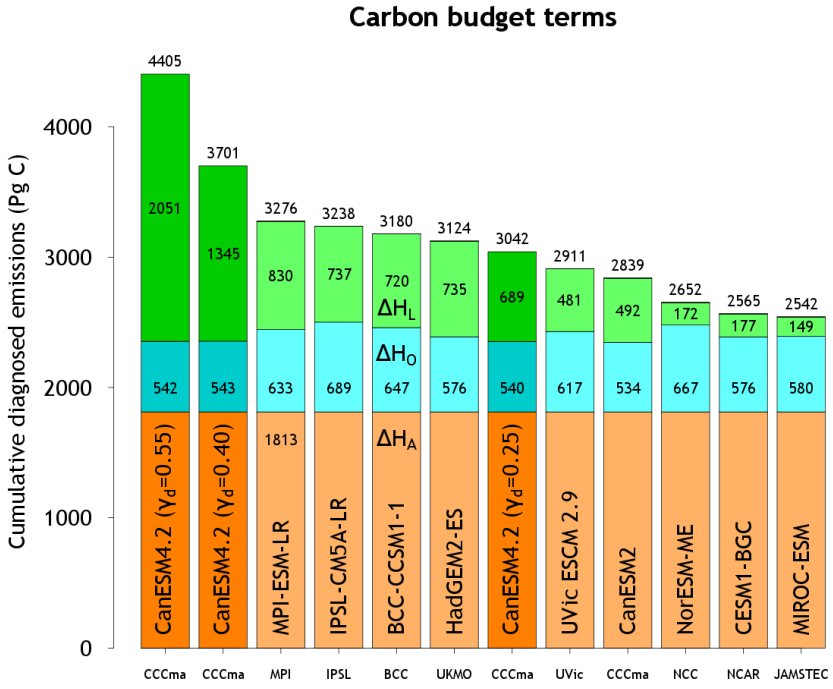

Figure 2. Components of the carbon budget Eq. (8) that make up cumulative diagnosed emissions based on results from the fully coupled 1pctCO2 experiment. Results shown are from eight CMIP5 models that participated in the Arora et al. (2013) study and from three CanESM4.2 simulations (shown in darker colours) for three different strengths of the terrestrial CO_2 fertilization effect.

Table 1. Summary of simulations performed for this study and the forcings used.

Simulation	1pctCO2	esmhistorical	esmhistorical_noluc
Simulation details	1 % per year increasing CO_2 simulation	1850–2005 historical simulation based on CMIP5 protocol	1850–2005 historical simulation based on CMIP5 protocol, but with no anthropogenic land use change
Purpose	To allow for comparison of CanESM4.2 with CMIP5 models especially in terms of its land carbon uptake	To compare simulated aspects of the global carbon cycle and historical carbon budget with observation-based estimates	To diagnose LUC emissions by differencing atmosphere–land CO_2 flux between historical simulations with and without LUC.
Length	140 years	156 years	
CO_2 forcing	285 ppm at the start of the simulation and 1140 ppm after 140 years.	Historical CO_2 forcing	
Land cover forcing	Land cover corresponds to its 1850 state	Land cover evolution is based on increase in crop area over the historical period	Land cover corresponds to its 1850 state
Non-CO_2 greenhouse gases (GHGs) forcing	Concentration of non-CO_2 GHGs is specified at their 1850 levels.	Concentration of non-CO_2 GHGs is specified and evolves over the historical period based on the CMIP5 protocol	
Aerosols forcing	Emissions of aerosols and their precursors are specified at their 1850 levels.	Emissions of aerosols and their precursors are specified and evolve over the historical period based on the CMIP5 protocol	

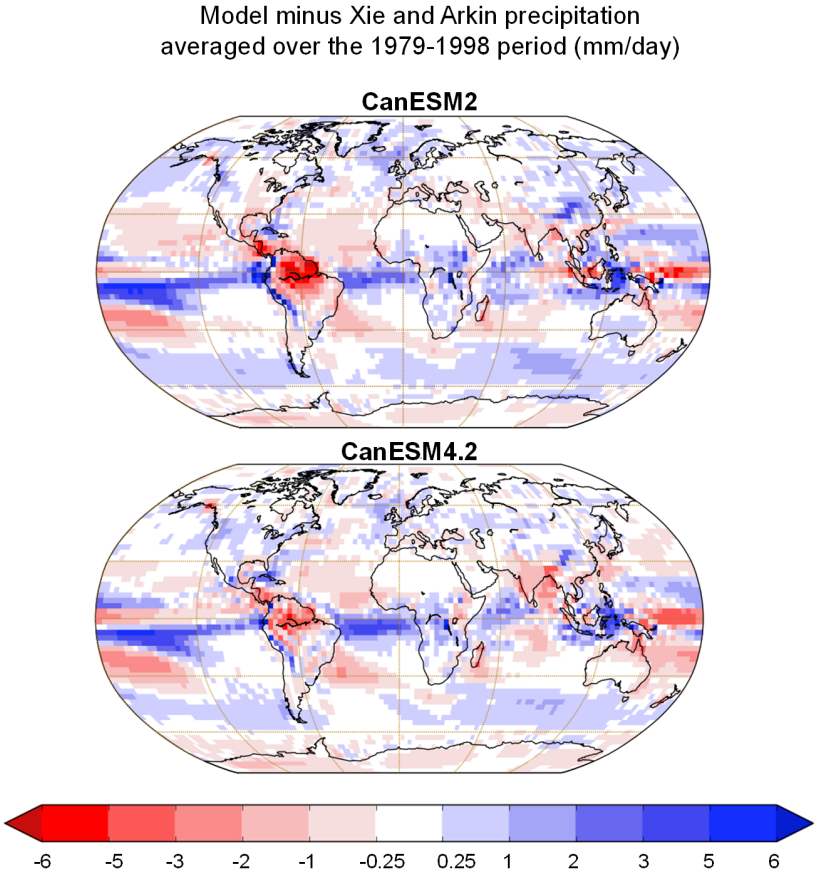

Figure 3. CanESM2 (panel **a**) and CanESM4.2 (panel **b**; $\gamma_d = 0.40$) precipitation anomalies compared to the observation-based estimates from CPC Merged Analysis of Precipitation (CMAP) based on Xie and Arkin (1997) averaged over the 1979–1998 period.

4 Results

4.1 1 % per year increasing CO_2 experiments

Figure 2 shows the carbon budget components of Eq. (8); ΔH_A, ΔH_O, and ΔH_L, i.e. the change in atmospheric carbon burden and cumulative atmosphere–ocean and atmosphere–land CO_2 flux, which together make up the cumulative diagnosed emissions ($\widetilde{E}$) based on results from the fully coupled 1pctCO2 experiment. Results are shown from eight CMIP5 models that participated in the Arora et al. (2013) study, including CanESM2, which used $\gamma_d = 0.25$, together with those from CanESM4.2 for three different strengths of the terrestrial CO_2 fertilization effect. The cumulative atmosphere–land CO_2 flux across models varies much more than the cumulative atmosphere–ocean CO_2 flux across the CMIP5 models as already noted in Arora et al. (2013). The results for CanESM4.2 indicate that the influence of γ_d (Eq. 12) on the strength of the model's terrestrial CO_2 fertilization effect allows CanESM4.2's cumulative diagnosed emissions to essentially span the range of the other CMIP5 models. For the three different strengths of the terrestrial CO_2 fertilization effect, $\gamma_d = 0.25$, 0.4, and 0.55, the γ_d values of 0.4 and 0.55 yield cumulative atmosphere–land CO_2 flux that is higher than all the CMIP5 models. The basis for choosing these values of γ_d within the range 0.4 ± 0.15 is that they span the observation-based estimates of various quantities reasonably well as shown later.

The cumulative atmosphere–land CO_2 flux ΔH_L for CanESM4.2 for the simulation with $\gamma_d = 0.25$ is higher than that for CanESM2, which also uses $\gamma_d = 0.25$, because of the changes made to soil moisture sensitivity of photosynthesis and because ΔH_L also depends on the model climate. In particular, the CanESM2 bias of low precipitation over the Amazonian region has been reduced in CanESM4.2, as shown in Fig. 3. The increased precipitation over the Amazonian region causes increased carbon uptake with increasing [CO_2]. The improved precipitation bias of CanESM4.2 in this region is in part caused by the decreased sensitivity of photosynthesis to soil moisture in CTEM4.2, especially for broadleaf evergreen PFT, which helps to increase evapotranspiration and in turn increase precipitation over the region.

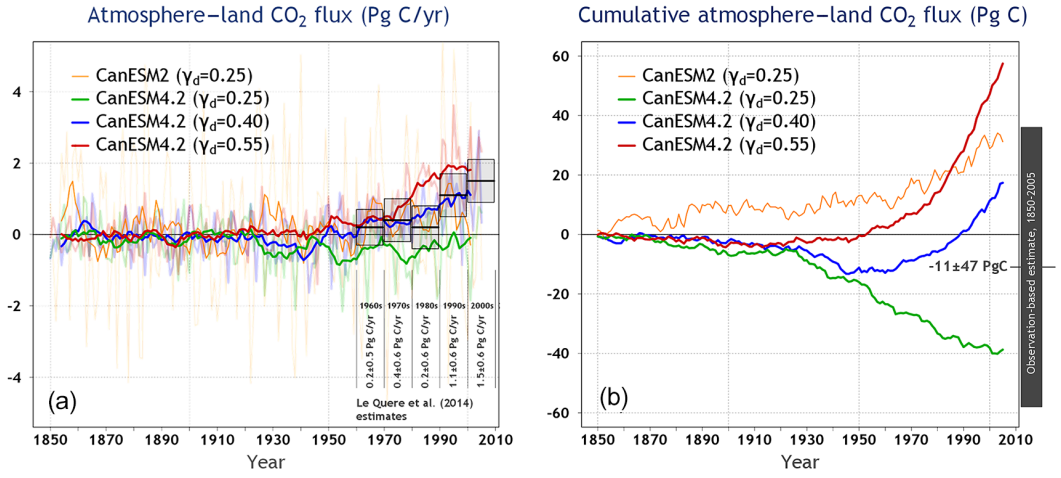

Figure 4. Atmosphere–land CO_2 flux (F_L) **(a)** and its cumulative values $\widetilde{F}_L$ **(b)** from CanESM2 and the three CanESM4.2 historical 1850–2005 simulations for different strengths of the terrestrial CO_2 fertilization effect. In **(a)** the observation-based estimates of F_L and their uncertainty (shown via boxes) for the decades of 1960, 1970, 1980, 1990, and 2000 are reproduced from Le Quéré et al. (2015). The bold lines in **(a)** are the 10-year moving averages of the annual F_L values, which are shown in light colours. The results from CanESM2 and CanESM4.2 are the average of the two ensemble members.

4.2 Historical simulations with LUC

The results presented in this section evaluate the model against four observation-based determinants of the global carbon cycle and the historical global carbon budget over the 1850–2005 period mentioned earlier. Simulated atmosphere–ocean CO_2 fluxes are also compared with observation-based estimates although, of course, they are not directly affected by the strength of the terrestrial CO_2 fertilization effect.

4.2.1 Components of land carbon budget

In Fig. 4, time series of instantaneous (F_L panel a) and cumulative ($\widetilde{F}_L$ panel b) atmosphere–land CO_2 flux over the period 1850–2005 are displayed for CanESM2 (which contributed results to CMIP5) and CanESM4.2 for the three different strengths of the terrestrial CO_2 fertilization effect. The observation-based estimates of $F_L = (F_l - E_L)$ in Fig. 4a for the decades of 1960, 1970, 1980, 1990, and 2000 are reproduced from Le Quéré et al. (2015), who derive the $F_L = (F_l - E_L)$ term as residual of the carbon budget equation $dH_A/dt = -(F_l - E_L) - F_O + E_F$ using observation-based estimates of change in atmospheric carbon budget (dH_A/dt), atmosphere–ocean CO_2 flux (F_O) and fossil fuel emissions (E_F). The observation-based estimate of -11 ± 47 Pg C in Fig. 4b for $\widetilde{F}_L$ over the period 1850–2005 is from Arora et al. (2011) (their Table 1).

The primary difference between CanESM2 and CanESM4.2 simulations in Fig. 4 is that $\widetilde{F}_L$ for CanESM2 generally stays positive throughout the historical period, whereas for CanESM4.2 it first becomes negative (indicating that land is losing carbon) and then becomes positive (indicating that land is gaining carbon) towards the end of the 20th century, depending on the strength of the CO_2 fertilization effect. The behaviour of $\widetilde{F}_L$ for CanESM4.2 is considered to be more realistic. As the land responds to anthropogenic land use change, associated with an increase in crop area early in the historical period, it causes a decrease in vegetation and soil carbon (see Fig. 5). Later in the 20th century, the CO_2 fertilization effect causes the land to become a sink for carbon resulting in both vegetation and soil carbon increases. This behaviour is consistent with the mean model response of the 15 CMIP5 models analysed by Hoffman et al. (2013) (their Fig. 2b). In contrast, CanESM2 shows a gradual increase in the global soil carbon amount (Fig. 5a) over the historical period. In Fig. 5, it can be seen that the effect of CO_2 fertilization in the second half of the 20th century is delayed for soil carbon compared to that for vegetation. This is primarily because of the lag introduced by the turnover time of vegetation (i.e. increased NPP inputs have to go through vegetation pool first) and the longer turnover timescale of the soil carbon pool. The more reasonable response of soil carbon to anthropogenic land use change, in Fig. 5a for CanESM4.2, is achieved by changing the humification factor from 0.45 (in CanESM2) to 0.10 (in CanESM4.2) in Eq. (5), which yields a reduction in global soil carbon amount in response to land use change up until the time that the effect of CO_2 fertilization starts to take effect. In Fig. 4a, CanESM4.2 is also able to simulate continuously increasing F_L during the period 1960 to 2005, depending on the strength of the CO_2 fertilization effect, whereas CanESM2 simulates near constant or decreasing F_L from about 1990 onwards, as is also seen in Fig. 4b for $\widetilde{F}_L$. This behaviour of F_L is not consistent with observation-

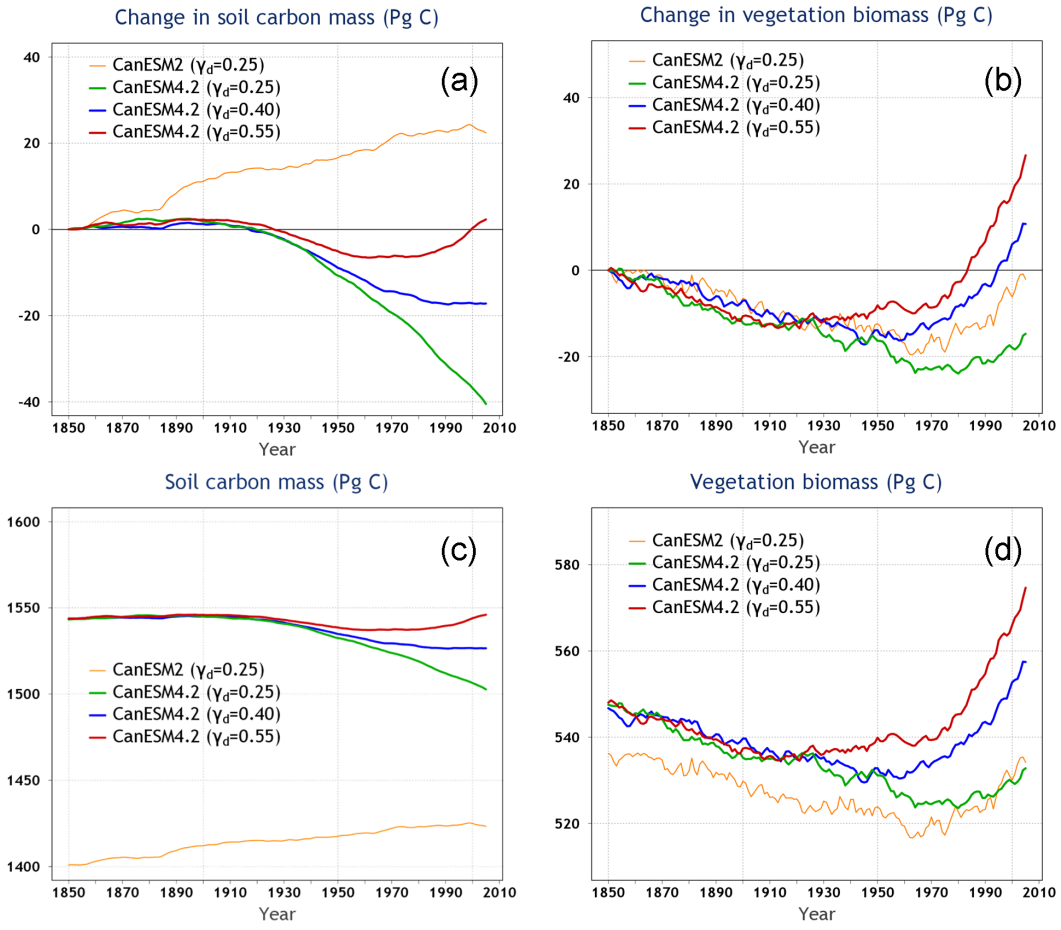

Figure 5. Change in and absolute values of global soil carbon and vegetation biomass amounts from CanESM2 and the three CanESM4.2 historical 1850–2005 simulations with different strengths of the terrestrial CO_2 fertilization effect. The results shown in all panels are the average of the two ensemble members.

based estimates from Le Quéré et al. (2015), which show continued strengthening of the land carbon sink since 1960s.

In Fig. 4a, amongst the three versions of the CanESM4.2, the simulation with $\gamma_d = 0.4$ (blue line) yields the best comparison with observation-based estimates of F_L from Le Quéré et al. (2015), while the simulations with $\gamma_d = 0.25$ (green line) and $\gamma_d = 0.55$ (red line) yield F_L values that are lower and higher, respectively, than observation-based estimates. In Fig. 4b, the cumulative atmosphere–land CO_2 flux $\widetilde{F}_L$ over the 1850–2005 period from the simulations with $\gamma_d = 0.25$ and 0.4 (green and blue lines, respectively) lies within the uncertainty of observation-based estimates, while the simulation with $\gamma_d = 0.55$ (red line) yields $\widetilde{F}_L$ value that is high relative to observation-based estimate.

Figure 6 shows the change in and absolute values of NPP from CanESM2 and the simulations made with CanESM4.2 for three different strengths of the CO_2 fertilization effect. Consistent with 1pctCO2 simulations, the rate of increase of NPP in CanESM4.2 with $\gamma_d = 0.25$ is higher than that in CanESM2, which also uses $\gamma_d = 0.25$. This is because the underlying model climate is different in CanESM2 and CanESM4.2, as mentioned earlier, and the fact that photosynthesis sensitivity to soil moisture has also been reduced. The rates of increase of NPP for $\gamma_d = 0.40$ and 0.50 are, of course, even higher. The CanESM4.2 simulation with $\gamma_d = 0.40$, which yields the best comparison with observation-based estimates of F_L for the decade of 1960 through 2000 (Fig. 4a) as well as $\widetilde{F}_L$ for the period 1850–2005 (Fig. 4b), yields an increase in NPP of ~ 16 Pg C year^{-1} over the 1850–2005 period. A caveat here is that part of this increase is also caused by increase in the crop area over the historical period that is realized in the model regardless of the strength of the CO_2 fertilization effect. In CTEM, the maximum photosynthetic capacity of crops is higher than for other PFTs to account for the fact that agricultural areas are generally fertilized. As a result, increase in crop area also increases global NPP. The increasing crop productivity has been suggested to contribute to the increase in amplitude of the annual $[CO_2]$ cycle since 1960s (Zeng et al., 2014). However, in the absence of an explicit representation of terrestrial N

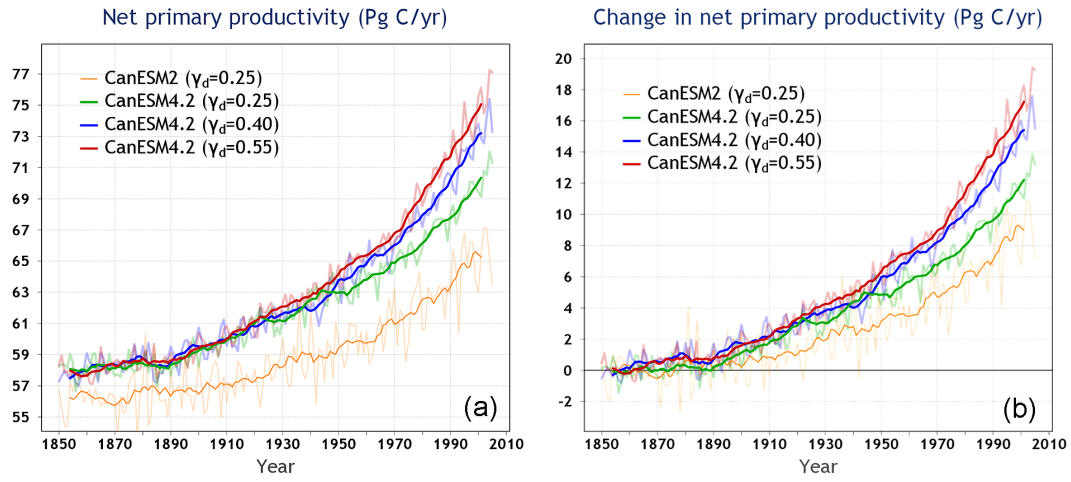

Figure 6. Absolute values of **(a)** and change in **(b)** net primary productivity (NPP) from CanESM2 and the three CanESM4.2 historical 1850–2005 simulations with different strengths of the terrestrial CO_2 fertilization effect. The thin lines show the ensemble-mean based on results from the two ensemble members and the bold lines are their 10-year moving averages.

cycle (and thus fertilization of cropped areas) or a representation of increase in crop yield per unit area due to genetic modifications, the only processes in CTEM that contribute to changes in crop yield are the change in crop area itself and the increase in crop NPP due to the CO_2 fertilization effect.

4.2.2 Globally averaged [CO_2]

Figure 7 shows the simulated globally averaged surface [CO_2] from the emissions-driven esmhistorical simulation of CanESM2 and that of CanESM4.2 for three different strengths of the CO_2 fertilization effect. The observation-based time series of [CO_2] is illustrated by the heavy black line. The CanESM2 ($\gamma_d = 0.25$) simulation yields a reasonable comparison with observation-based [CO_2]. Amongst the versions of CanESM4.2 with different strengths of the CO_2 fertilization effect, the version with $\gamma_d = 0.40$ yield the best comparison. The CanESM4.2 version with $\gamma_d = 0.25$ (weaker strength of the CO_2 fertilization effect) and 0.55 (stronger CO_2 fertilization effect) yield CO_2 concentrations that are respectively higher and lower than the observational estimate from roughly mid-20th century onward. The reason CanESM4.2 ($\gamma_d = 0.40$) requires a stronger CO_2 fertilization effect than CanESM2 ($\gamma_d = 0.25$) for simulating the observation-based increase in atmospheric CO_2 burden over the historical period is the enhanced impact of LUC in CanESM4.2 due to its increased humification factor and the associated response of the global soil carbon pool, as discussed in the previous section. The differences in simulated [CO_2] in Fig. 7 from CanESM4.2 are due only to differences in the strength of the CO_2 fertilization effect. Although, of course, since in these simulations [CO_2] is simulated interactively, the simulated atmosphere–land flux F_L and [CO_2] both respond to and affect each other.

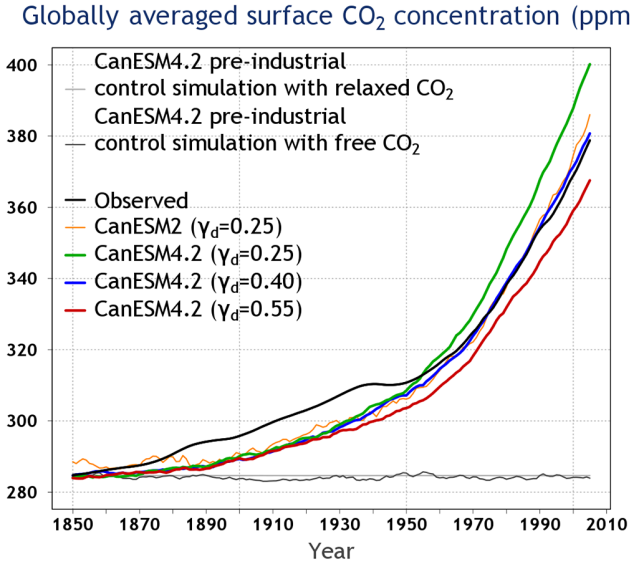

Figure 7. Simulated globally averaged surface atmospheric CO_2 concentration from CanESM2 and the three CanESM4.2 historical 1850–2005 simulations with different strengths of the terrestrial CO_2 fertilization effect. The observation-based concentration is shown in black. Also shown is the CO_2 concentration of 284.6 ppm used in CanESM4.2's pre-industrial simulation in the relaxed-CO2 configuration and the simulated concentration from the pre-industrial CanESM4.2 simulation with interactively determined CO_2.

Both CanESM2 and CanESM4.2 underpredict [CO_2] relative to observational estimates over the period 1850–1930, and are also unable to reproduce the near-zero rate of increase of [CO_2] around 1940. Possible reasons for these discrepancies include (1) the possibility that the carbon cycle

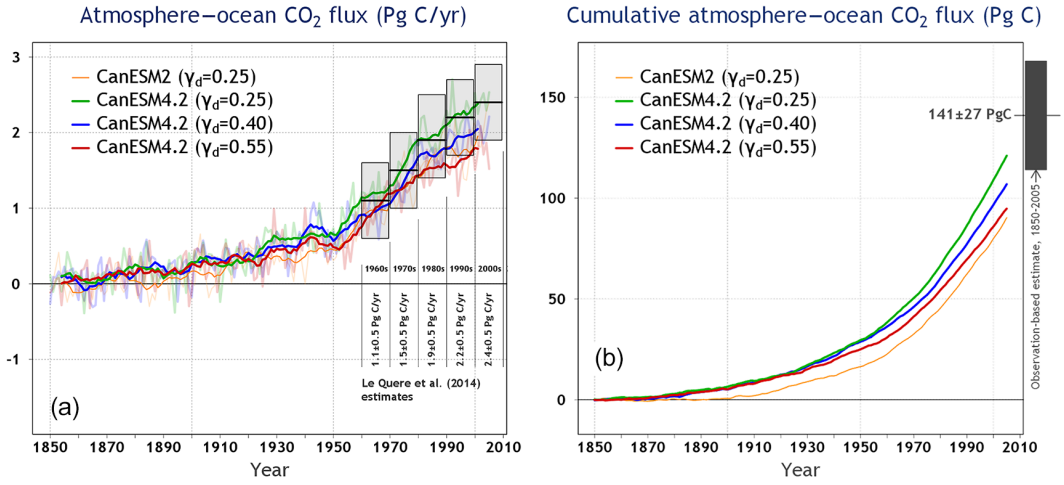

Figure 8. Atmosphere–ocean CO_2 flux (F_O) **(a)** and its cumulative values $\widetilde{F}_O$ **(b)** from CanESM2 and the three CanESM4.2 historical 1850–2005 simulations for three different strengths of the terrestrial CO_2 fertilization effect. In **(a)** the observation-based estimates of F_O and their uncertainty (show via boxes) for the decades of 1960, 1970, 1980, 1990, and 2000 are reproduced from Le Quéré et al. (2015). The bold lines in **(a)** are the 10-year moving averages of the annual F_L values, which are shown in light colours. The results from CanESM2 and CanESM4.2 are the average of the two ensemble members.

before 1850 was not in true equilibrium and this aspect cannot be captured since the model is spun up to equilibrium for 1850 conditions, (2) the uncertainties associated with anthropogenic emissions for the late 19th and early 20th century that are used to drive the model, and (3) the uncertainties associated with pre-Mauna Loa [CO_2] observations.

4.2.3 Atmosphere–ocean CO_2 flux

Figure 8a and b, respectively, show time series of instantaneous (F_O) and cumulative ($\widetilde{F}_O$) atmosphere–ocean CO_2 fluxes over the period 1850–2005 for the set of emissions-driven simulations presented in Fig. 7. The strength of the terrestrial CO_2 fertilization effect has little or no impact on the ocean biogeochemical processes. The differences in values of F_O and $\widetilde{F}_O$ for the three versions CanESM4.2 are, therefore, primarily due to the differences in [CO_2]. The observation-based estimates of F_O in Fig. 8a for the decades of 1960, 1970, 1980, 1990, and 2000 are from Le Quéré et al. (2015). The observation-based estimate of $\widetilde{F}_O$ of 141 ± 27 Pg C in Fig. 8b for the period 1850–2005 is from Arora et al. (2011) (their Table 1).

Both CanESM2 and the CanESM4.2 simulation for $\gamma_d = 0.40$ (which provides the best comparison with observation-based estimate for [CO_2]; blue line in Fig. 7) yield lower $\widetilde{F}_O$ compared to observation-based values. The F_O value from CanESM2 and the CanESM4.2 simulation for $\gamma_d = 0.40$ are lower than the mean estimates from Le Quéré et al. (2015) for the decades of 1960s through 2000s, although still within their uncertainty range. The family of ESMs from CCCma, all of which have the same physical ocean model, including CanESM1 (Arora et al., 2009), CanESM2 (Arora et al., 2011) and now CanESM4.2, yield lower than observed ocean carbon uptake over the historical period. Recent analyses of these model versions suggest that the primary reason for their low carbon uptake is a negative bias in near-surface wind speeds over the Southern Ocean and an iron limitation in the same region, which is too strong (personal communication, Neil Swart, Canadian Centre for Climate Modelling and Analysis). The CanESM4.2 simulation with $\gamma_d = 0.25$ (green line in Fig. 8) yields a better comparison with observation-based estimates of F_O and $\widetilde{F}_O$ but that is because of the higher simulated [CO_2] in that simulation associated with lower carbon uptake by land.

4.2.4 Amplitude of the annual CO_2 cycle

The annual CO_2 cycle is influenced strongly by the terrestrial biospheric activity of the Northern Hemisphere (Keeling et al., 1996; Randerson et al., 1997). Higher than normal biospheric uptake of carbon during a Northern Hemisphere's growing season, for example, will yield lower than normal [CO_2] by the end of the growing season, around September when [CO_2] is at its lowest level (see Fig. 9a). Similarly, during the Northern Hemisphere's dormant season, increased respiration from live vegetation and decomposition of dead carbon, including leaf litter, that may be associated with increased carbon uptake during the last growing season, will yield higher than normal [CO_2] during April when [CO_2] is at its highest level. Both processes increase the amplitude of the annual [CO_2] cycle. Given this strong control, the rate of change of the amplitude of the annual [CO_2] cycle can potentially help to constrain the strength of the terrestrial CO_2 fertilization effect.

Figure 9a compares the annual cycle of the trend-adjusted globally averaged near-surface monthly [CO_2] anomalies from CanESM2 and the versions of CanESM4.2 for three different strengths of the CO_2 fertilization effect with observation-based estimates for the 1991–2000 period. Figure 9b shows the time series of the amplitude of the annual cycle of the trend-adjusted globally averaged near-surface monthly [CO_2] anomalies (referred to as Φ_{CO_2}) from CanESM2 and CanEM4.2, as well as observation-based estimates going back to 1980s. While CO_2 measurements at Mauna Loa started in 1959, observation-based globally averaged near-surface [CO_2] values are only available since 1980s (ftp://aftp.cmdl.noaa.gov/products/trends/co2/co2_mm_gl.txt). In Fig. 9b, consistent with the strengthening of the CO_2 fertilization effect, associated with the increase in [CO_2], the observation-based estimate of Φ_{CO_2} shows an increase from 1980s to the present. Both CanESM2 and versions of CanESM4.2 also show an increase in the amplitude of Φ_{CO_2} over the period 1850–2005. However, the absolute values of Φ_{CO_2} are lower in CanESM2 than in CanESM4.2 (Fig. 9b). Of course, in the absence of an observation-based estimate of pre-industrial value of Φ_{CO_2} it is difficult to say which value is more correct. However, when considering the present-day values of Φ_{CO_2}, the three versions of CanESM4.2 yield better comparison with observation-based estimate as also shown in Fig. 9a. The increase in the value of Φ_{CO_2} from CanESM2 to CanESM4.2, which now yields better comparison with observation-based value of Φ_{CO_2}, is most likely caused by the change in the land surface scheme from CLASS 2.7 (that is implemented in CanESM2) to CLASS 3.6 (implemented in CanESM4.2), since the atmospheric component of the model has not changed substantially. It is, however, difficult to attribute the cause of this improvement in the present-day value of Φ_{CO_2} in CanESM4.2 to a particular aspect of the new version of the land surface scheme. The annual [CO_2] cycle is driven primarily by the response of the terrestrial biosphere to the annual cycle of temperature and the associated greening of the biosphere every summer in the Northern Hemisphere. However, the simulated amplitude of the annual cycle of near-surface temperature has not changed substantially from CanESM2 to CanESM4.2 (not shown).

In Fig. 9b, the simulated values of Φ_{CO_2} for the CanESM4.2 simulations with $\gamma_d = 0.25$, 0.40, and 0.55 are 4.41, 4.69, and 4.85 ppm, respectively, averaged over the period 1991–2000, compared to observation-based value of Φ_{CO_2} of 4.36 ppm. Here, CanESM4.2 simulation with $\gamma_d = 0.25$ yields the best comparison with observation-based value of Φ_{CO_2}. An increase in the strength of the CO_2 fertilization effect increases the amplitude of the annual [CO_2] cycle so a larger value of γ_d yields a larger value of Φ_{CO_2}. The increase in the amplitude of the annual [CO_2] cycle comes both from lower [CO_2] at the end of the growing season in September as well as higher [CO_2] at the start of the Northern Hemisphere's growing season in April (see Fig. 9a), as mentioned earlier in this section.

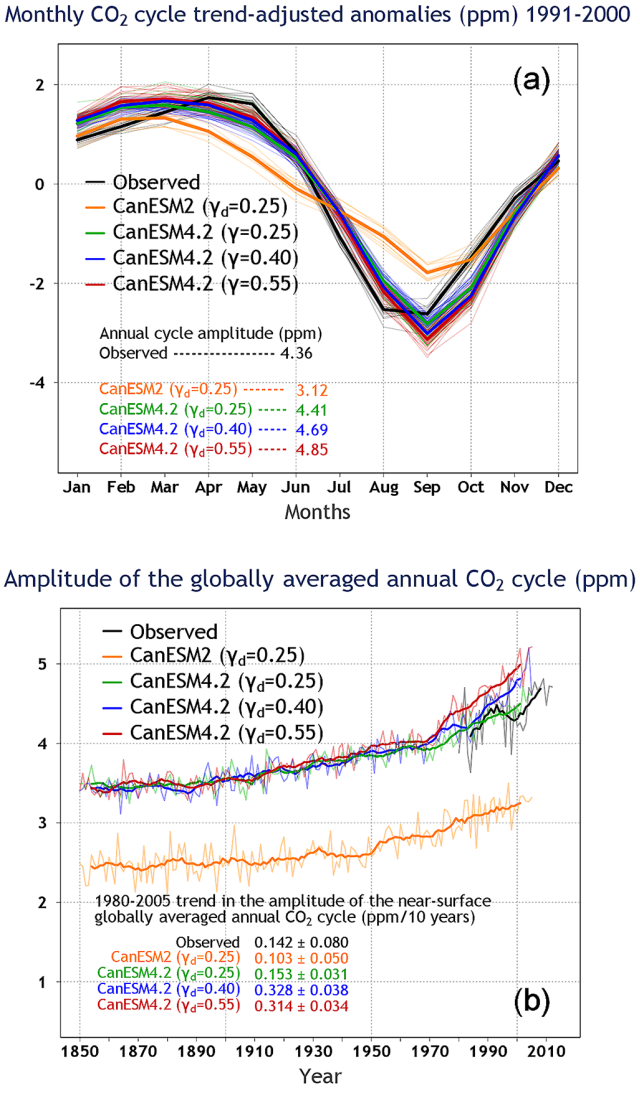

Figure 9. The annual cycle of trend-adjusted globally averaged near-surface monthly [CO_2] anomalies from CanESM2, the versions of CanESM4.2 for three different strengths of the CO_2 fertilization effect and observation-based estimates for the 1991–2000 period **(a)**. Panel **(b)** shows the time series of the amplitude of the annual cycle of the trend-adjusted globally averaged near-surface monthly [CO_2] anomalies for corresponding model and observation-based estimates. The bold lines are 10-year moving averages and the thin lines for model results are the average of results from two ensemble members.

More important than the absolute value of Φ_{CO_2} is its rate of increase over time, which is a measure of the strength of the terrestrial CO_2 fertilization effect. Figure 9b also shows the trend in Φ_{CO_2} over the 1980–2005 overlapping period for which for both the model and observation-based estimates of Φ_{CO_2} are available. The magnitude of trend for

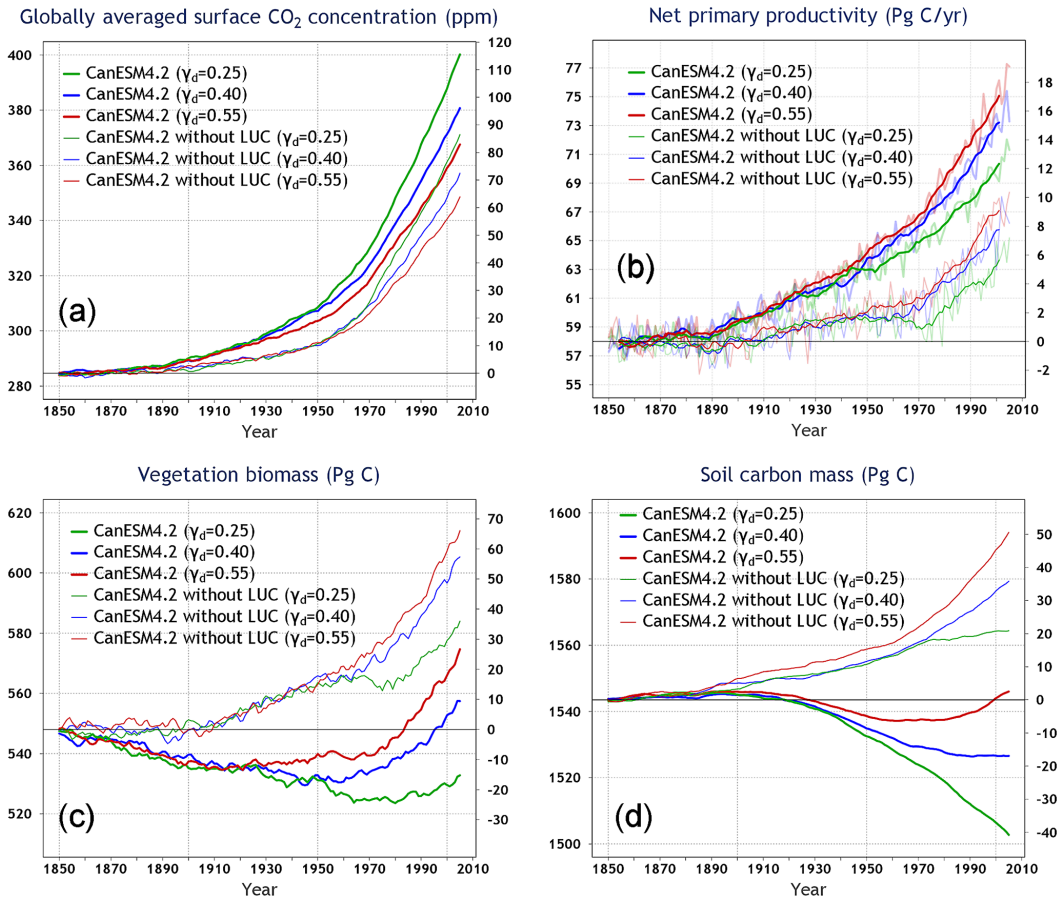

Figure 10. Comparison of CanESM4.2 simulations with and without implementation of anthropogenic land use change over the historical period for three different strengths of the terrestrial CO_2 fertilization effect: **(a)** globally averaged annual surface atmospheric CO_2 concentration, **(b)** net primary productivity, **(c)** global vegetation biomass, and **(c)** global soil carbon mass. All lines are the average of results from two ensemble members. Additionally, in **(b)** the bold lines are the 10-year moving averages.

observation-based estimate of Φ_{CO_2} is 0.142 ± 0.08 ppm 10-years^{-1} (mean $\pm$ standard deviation, $\bar{x} \pm \sigma_x$), implying that over the 26-year 1980–2005 period the amplitude of annual $[CO_2]$ cycle has increased by 0.37 ± 0.21 ppm. The calculated mean and standard deviation of the observation-based trend, however, does not take into account the uncertainty associated with the observation-based estimates of $[CO_2]$, consideration of which will increase the calculated standard deviation even more. The magnitudes of trend in Φ_{CO_2} simulated by CanESM2 ($\gamma_d = 0.25$) and CanESM4.2 (for $\gamma_d = 0.25$) are 0.103 ± 0.05 and 0.153 ± 0.031, respectively, and statistically not different from the trend in the observation-based value of Φ_{CO_2} implying an increase of 0.27 ± 0.13 and 0.40 ± 0.08 ppm, respectively, in Φ_{CO_2} over the 1980–2005 period. The statistical difference is calculated on the basis of $\bar{x} \pm 1.385\sigma_x$ range, which corresponds to 83.4 % confidence intervals; the estimates from two sources are statistically not different at the 95 % confidence level if this range overlaps (Knol et al., 2011). The magnitudes of the trend in Φ_{CO_2} over the 1980–2005 period for CanESM4.2 simulations with $\gamma_d = 0.4$ and 0.55 (0.328 ± 0.038 and 0.314 ± 0.034 ppm 10-years^{-1}, respectively) are, however, more than twice, as well as statistically different from, the observation-based estimate (0.142 ± 0.08 ppm 10-years^{-1}).

Overall, the CanESM4.2 simulation with $\gamma_d = 0.25$ yields the amplitude of the globally average annual CO_2 cycle and its rate of increase over the 1980–2005 period that compares best with observation-based estimates.

4.3 Historical simulations without LUC

Figures 10 and 11 show results from CanESM4.2 emissions-driven simulations for three different strengths of the CO_2 fertilization effect that do not implement anthropogenic LUC over the historical period and compare them to their corresponding simulations with LUC.

Figure 10a compares the simulated $[CO_2]$; as expected in the absence of anthropogenic LUC the simulated $[CO_2]$ is lower since LUC emissions do not contribute to increase in $[CO_2]$. The difference in $[CO_2]$ at the end of the simulation,

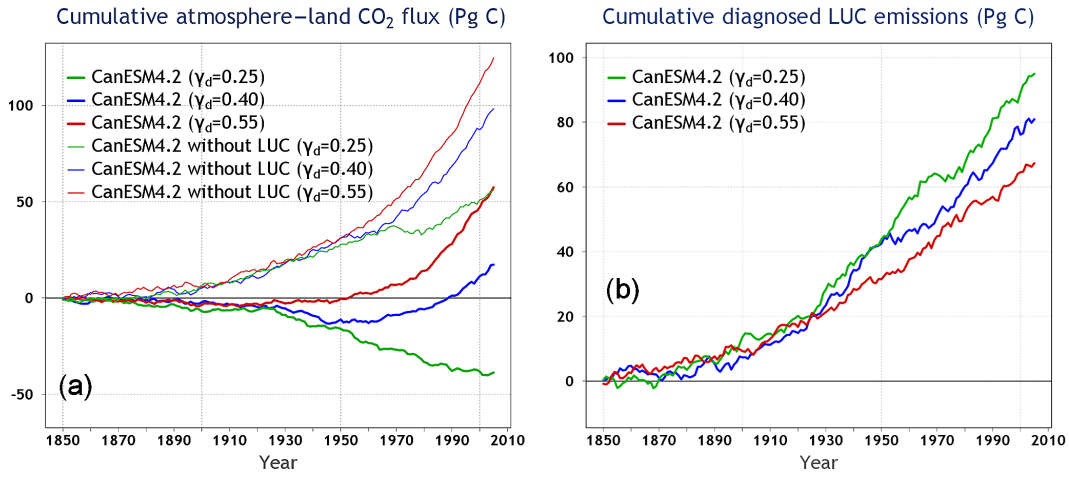

Figure 11. Comparison of simulated cumulative atmosphere–land CO_2 flux from CanESM4.2 simulations with and without implementation of anthropogenic land use change over the historical period for three different strengths of the terrestrial CO_2 fertilization **(a)**. Panel **(b)** shows the cumulative diagnosed LUC emissions calculated using Eq. (10) as the difference between cumulative atmosphere–land CO_2 flux from simulations with and without LUC shown in **(a)**. All lines are the average of results from two ensemble members.

in year 2005, between simulations with and without LUC is 29.0, 23.6, and 19.0 ppm for $\gamma_d = 0.25$, 0.40, and 0.55. The simulations with the lowest strength of the CO_2 fertilization effect ($\gamma_d = 0.25$) yield the largest difference because these simulations also have the largest [CO_2] amongst their set of simulations with and without LUC. The CO_2 fertilization of the terrestrial biosphere implies that the effect of deforestation will be higher, because of reduced carbon uptake by deforested vegetation, if background [CO_2] is higher.

Figure 10b compares the simulated NPP from CanESM4.2 simulations with and without LUC. The increase in simulated NPP, regardless of the strength of the CO_2 fertilization effect, is lower over the historical period in simulations without LUC for two apparent reasons. First, the rate of increase of [CO_2] is itself lower and second, in the absence of LUC, there is no contribution from increasing crop area to NPP. Overall, the increase in NPP over the 1850–2005 period in simulations with LUC is a little more than twice that in simulations without LUC. Figure 10c and d compare the changes in global vegetation biomass and soil carbon mass, over the historical period, from simulations with and without LUC. As expected, in the absence of LUC, global vegetation biomass, and soil carbon mass more or less show a continuous increase, associated with the increase in NPP, which itself is due to the increase in [CO_2]. Consequently, in Fig. 11a, the cumulative atmosphere–land CO_2 flux $\widetilde{F}_L$ in simulations without LUC also shows a more or less continuous increase over the historical period.

Finally, Fig. 11b shows the diagnosed cumulative LUC emissions $\widetilde{E}_L$ calculated as the difference between cumulative $\widetilde{F}_L$, following Eq. (10), from simulations with and without LUC. The diagnosed $\widetilde{E}_L$ in this manner are equal to 95, 81, and 67 Pg C, over the 1850–2005 period, for $\gamma_d = 0.25$, 0.40, and 0.55. The calculated diagnosed $\widetilde{E}_L$ are highest for $\gamma_d = 0.25$ associated with the highest background simulated [CO_2] in these simulations, as mentioned earlier. For comparison, LUC emissions estimated by Houghton (2008) for the period 1850–2005, based on a bookkeeping approach, are 156 Pg C but these estimates are generally believed to be ±50 % uncertain (see Fig. 1 of Ramankutty et al., 2007). LUC emissions, when calculated by differencing F_L from simulations with and without LUC, also depend on the type of simulations performed – in particular, if simulations are driven with specified CO_2 concentrations or specified CO_2 emissions. Had our simulations been concentration driven, in contrast to being emissions driven, then both with and without LUC simulations would have experienced the same specified observed CO_2 concentration over the historical period and the simulated LUC emissions would have been higher. Arora and Boer (2010) found that diagnosed LUC emissions in the first version of the Canadian Earth system model (CanESM1) increased from 71 Pg C (for emissions-driven simulations) to 124 Pg C (for concentration-driven simulations). Concentration-driven simulations, however, cannot be evaluated against observation-based amplitude of the annual CO_2 cycle and its increase over the historical period. These simulations either ignore the annual cycle of CO_2 (our specified-CO2 case) or use a specified amplitude of the CO_2 annual cycle (our relaxed-CO2 case).

5 Discussion and conclusions

This study evaluates the ability of four observation-based determinants of the global carbon cycle and the historical carbon budget to constrain the parameterization of photosynthesis down-regulation, which directly determines the

strength of the CO_2 fertilization effect, over the historical period 1850–2005. The key parameter that controls the strength of the CO_2 fertilization effect in CTEM, γ_d, was varied in the latest version of CCCma's Earth system model CanESM4.2. Comparing simulated and observation-based estimates of (1) globally averaged atmospheric CO_2 concentration, (2) cumulative atmosphere–land CO_2 flux, and (3) atmosphere–land CO_2 flux for the decades of 1960s, 1970s, 1980s, 1990s, and 2000s, it is found that the CanESM4.2 version with $\gamma_d = 0.40$ yields the best comparison.

The evaluation of CTEM within the framework of CanESM4.2 presented here is based on an emergent model property at the global scale and may be considered as a top-down approach of model evaluation. In contrast, the bottom-up approaches of model evaluation typically evaluate model results and processes against observations of primary atmosphere–land carbon and/or nitrogen fluxes and sizes of the vegetation, litter and soil carbon/nitrogen pools (e.g. Zaehle et al., 2014). Indeed, CTEM has been evaluated at point (e.g. Arora and Boer, 2005; Melton et al., 2015), regional (e.g. Peng et al., 2014; Garnaud et al., 2014), and global (e.g. Arora and Boer, 2010; Melton and Arora, 2014) scales in a number of studies when driven with observation-based reanalysis data. Both top-down and bottom-up approaches of model evaluation are complimentary to each other and allow to evaluate different aspects of the model at different spatial and temporal scales.

For the top-down approach used here, CanESM4.2 simulates globally averaged near-surface [CO_2] of 400, *381* and 368 ppm for $\gamma_d = 0.25$, *0.40*, and 0.55, respectively, compared to the observation-based estimate of *379* ppm for year 2005. The cumulative atmosphere–land CO_2 flux of 18 Pg C for the period 1850–2005 for $\gamma_d = 0.40$ lies within the range of the observation-based estimate of -11 ± 47 Pg C in Fig. 4b, and so do the average atmosphere–land CO_2 flux for the decades of 1960s through to 2000s in Fig. 4a when compared to observation-based estimates from Le Quéré et al. (2015). $\gamma_d = 0.25$ and 0.55 yield average atmosphere–land CO_2 flux for the decades of 1960s through to 2000s that are lower and higher, respectively, than the observation-based estimates from Le Quéré et al. (2015). The only determinant against which $\gamma_d = 0.40$ does not yield the best comparison with observation-based estimates is the amplitude of the globally averaged annual CO_2 cycle and its increase over the 1980 to 2005 period. For this determinant, $\gamma_d = 0.25$ seems to yield the best comparison (Fig. 9). The value of $\gamma_d = 0.40$ that yields best overall comparison with observation-based determinants of the global carbon cycle and the historical carbon budget is also broadly consistent with Arora et al. (2009), who derived a value of $\gamma_d = 0.46$ based on results from FACE studies (as mentioned in Sect. 2.2.2).

The caveat with the analyses presented here, or for any model for that matter, is that the strength of the terrestrial CO_2 fertilization effect is dependent on the processes included in the model and the parameter values associated with them. The primary example of this is the adjustment to the humification factor in CTEM4.2, which leads to reduction in the global soil carbon amount as anthropogenic LUC becomes significant towards the mid-20th century. This response of soil carbon was not present in the model's configuration of CTEM and historical simulations made with CanESM2. The representation of soil carbon loss, in response to anthropogenic LUC in CanESM4.2, implies that a stronger CO_2 fertilization effect (or weaker photosynthesis down-regulation) should be required to reproduce realistic atmosphere–land CO_2 flux over the historical period and this was found to be the case in Fig. 4a. Despite this dependence on processes included in the model, the response of the land carbon cycle, over the historical period, to the two primary forcings of increased [CO_2] and anthropogenic land use change must be sufficiently realistic in the model to satisfy all the four determinants of the global carbon cycle and the historical global carbon budget.

The simulated loss in soil carbon in response to anthropogenic LUC over the historical period may also be assessed against observation-based estimates from Wei et al. (2014). Using data from 453 sites that were converted from forest to agricultural land, Wei et al. (2014) found that the soil organic carbon stocks decreased by an average of 43.1 ± 1.1 % for all sites. Based on the HYDE v3.1 data set from which the changes in crop area are derived (Hurtt et al., 2011), LUC as implemented in CanESM4.2 yields an increase in crop area from about 5 million km^2 in 1850 to about 15 million km^2 in 2005. Assuming an initial soil carbon amount of 10 kg C m^{-2} (see Fig. 2c of Melton and Arora, 2014) and an average 40 % decrease in soil carbon amount, based on Wei et al. (2014), implies that the increase in crop area of about 10 million km^2 over the historical period has likely yielded a global soil organic carbon loss of 40 Pg C. The loss in soil carbon in Fig. 5a is simulated to 18 Pg C for CanESM4.2 simulations with $\gamma_d = 0.40$, the simulation that yields the best comparison with observation-based determinants of the global carbon cycle and the historical carbon budget. This loss of 18 Pg C is expected to be less than the 40 Pg C because the model estimates also include an increase associated with the increase in NPP due to the CO_2 fertilization effect from non-crop areas. The effect of LUC on global soil carbon loss may also by estimated by differencing global soil carbon amounts from simulations with and without LUC from Fig. 10d at the end of the simulation in year 2005. For CanESM4.2 simulation with $\gamma_d = 0.40$, this amounts to around 50 Pg C. Both these estimates of soil carbon loss are broadly consistent with the back-of-the-envelope calculation of 40 Pg C soil carbon loss, based on Wei et al. (2014) estimates, indicating that the soil carbon loss simulated in response to anthropogenic LUC over the historical period is not grossly over or underestimated.

The CanESM4.2 simulation with $\gamma_d = 0.40$, however, fails to satisfy the rate of increase of the amplitude of the globally

averaged annual CO_2 cycle over the 1980–2005 period implying that there are still limitations in the model structure and/or parameter values. Of course, the fact that the amplitude of the globally averaged annual CO_2 cycle is also affected by the atmosphere–ocean CO_2 fluxes makes it more difficult to attribute the changes in the amplitude of the globally averaged annual CO_2 cycle solely to atmosphere–land CO_2 fluxes. Additionally, the increase in crop area as well as crop yield per unit area over the historical period have been suggested by Zeng et al. (2014) to contribute towards the observed increase in the amplitude of annual CO_2 cycle. Based on their sensitivity tests, Zeng et al. (2014) attributed 45, 29, and 26 percent of the observed increase in the seasonal-cycle amplitude of the CO_2 cycle to LUC, climate variability and change (including factors such as the lengthening of the growing season), and increased productivity due to CO_2 fertilization, respectively. Comparison of the rate of increase of NPP in CanESM4.2 experiments with and without LUC (Fig. 10b), as a measure of increase in the strength of the CO_2 fertilization effect, suggests that the contribution of anthropogenic LUC to the increase in the seasonal-cycle amplitude is 52 %, which is broadly consistent with the 45 % value obtained by Zeng et al. (2014).

While CanESM4.2 simulation with $\gamma_d = 0.40$ is able to simulate a realistic rate of increase of $[CO_2]$ over the period 1960 to 2005, the modelled atmosphere–ocean CO_2 fluxes for this and the CanESM2 version are lower than observational estimates of this quantity (Fig. 8). This implies that if the modelled atmosphere–ocean CO_2 flux were to increase and become more consistent with observation-based estimates then the modelled atmosphere–land CO_2 flux must decrease to still be able to yield sufficiently realistic rate of increase of $[CO_2]$. This implies that the strength of the terrestrial CO_2 fertilization effect should likely be somewhat lower than what is obtained by $\gamma_d = 0.40$ or the simulated atmosphere–land CO_2 flux is higher because of some other reason, most likely lower LUC emissions. Indeed, the required decrease in modelled atmosphere–land CO_2 flux is consistent with the fact that the modelled LUC emissions for $\gamma_d = 0.40$ (81 Pg C) are about half the estimate from Houghton (2008) (156 Pg C) with the caveat, of course, that Houghton's estimates themselves have an uncertainty of roughly ±50 %. The LUC module of CTEM currently only accounts for changes in crop area and does not take into account changes associated with pasture area given their ambiguous definition (pasture may or may not be grasslands). The model also does not take into account wood harvesting, which amongst other uses is also used as a biofuel. Treatment of these additional processes will increase modelled LUC emissions.

Although the CanESM4.2 simulation with $\gamma_d = 0.40$ satisfies three out of four constraints placed by the chosen determinants of the global carbon cycle and the historical carbon budget, and also simulates reasonable soil carbon loss in response to anthropogenic LUC, the model now yields the highest land carbon uptake, in the 1pctCO2 experiment, amongst the CMIP5 models that were compared by Arora et al. (2013) as seen in Fig. 2. Of course, the 1pctCO2 experiment is in no way indicative of models' performance over the historical period, nor is being an outlier amongst CMIP5 models a conclusive evaluation of CanESM4.2's land carbon uptake. However, it remains possible that the chosen determinants of the global carbon cycle and the historical carbon budget are not able to constrain the model sufficiently, given the especially large uncertainty associated with LUC emissions. Nevertheless, these observation-based constraints of the carbon cycle and historical carbon budget are essentially the only means to evaluate carbon-cycle aspects of the ESMs at the global scale, including the strength of the terrestrial CO_2 fertilization effect. In the near future, availability of model output from the sixth phase of CMIP (CMIP6) will allow for a comparison of the simulated aspects of the global carbon cycle and the historical carbon budget from ESMs to observations-based estimates for the 1850–2014 period. These data will allow for a comparison of the rate of increase of the amplitude of globally averaged surface $[CO_2]$ in models with observation-based estimates over a longer period. This should help better constrain the strength of the terrestrial CO_2 fertilization effect, as it is represented in models, in a somewhat more robust manner.

6 Source code and data availability

Source code for the complete CanESM4.2 model is an extremely complex set of FORTRAN subroutines, with C pre-processor (CPP) directives, which reside in CCCma libraries. Unix shell scripts process the model code for compilation based on CPP directives and several other switches (e.g. those related to free-CO2, specified-CO2, and relaxed-CO2 settings). As such, it is extremely difficult to make the full model code available. However, selected model subroutines related to specific physical and biogeochemical processes can be made available by either author (vivek.arora@canada.ca, john.scinocca@canada.ca) upon agreeing to Environment and Climate Change Canada's software licensing agreement available at http://collaboration.cmc.ec.gc.ca/science/rpn.comm/license.html. Data used to produce plots and figures can be obtained from the first author (vivek.arora@canada.ca).

Acknowledgements. We would like to thank Joe Melton and Neil Swart for providing comments on an earlier version of this paper. We also thank the three anonymous reviewers for their constructive and helpful comments.

Edited by: J. Kala

References

Arora, V. K. and Boer, G. J.: A parameterization of leaf phenology for the terrestrial ecosystem component of climate models, Glob. Change Biol., 11, 39–59, doi:10.1111/j.1365-2486.2004.00890.x, 2005.

Arora, V. K. and Boer, G. J.: Uncertainties in the 20th century carbon budget associated with land use change, Glob. Change Biol., 16, 3327–3348, 2010.

Arora, V. K. and Boer, G. J.: Terrestrial ecosystems response to future changes in climate and atmospheric CO_2 concentration, Biogeosciences, 11, 4157–4171, doi:10.5194/bg-11-4157-2014, 2014.

Arora, V. K., Boer, G. J., Christian, J. R., Curry, C. L., Denman, K. L., Zahariev, K., Flato, G. M., Scinocca, J. F., Merryfield, W. J., and Lee, W. G.: The effect of terrestrial photosynthesis down-regulation on the 20th century carbon budget simulated with the CCCma Earth System Model, J. Climate, 22, 6066–6088, 2009.

Arora, V. K., Scinocca, J. F., Boer, G. J., Christian, J. R., Denman, K. L., Flato, G. M., Kharin, V. V., Lee, W. G., and Merryfield, W. J.: Carbon emission limits required to satisfy future representative concentration pathways of greenhouse gases, Geophys. Res. Lett., 38, L05805, doi:10.1029/2010GL046270, 2011.

Arora, V. K., Boer, G. J., Friedlingstein, P., Eby, M., Jones, C. D., Christian, J. R., Bonan, G., Bopp, L., Brovkin, V., Cadule, P., Hajima, T., Ilyina, T., Lindsay, K., Tjiputra, J. F., and Wu, T.: Carbon-Concentration and Carbon-Climate Feedbacks in CMIP5 Earth System Models, J. Climate, 26, 5289–5314, 2013.

Bartlett, P. and Verseghy, D.: Modified treatment of intercepted snow improves the simulatedforest albedo in the Canadian Land Surface Scheme, Hydrol. Process., 29, 3208–3226, doi:10.1002/hyp.10431, 2015.

Bartlett, P. A., Mackay, M. D., and Verseghy, D. L.: Modified snow algorithms in the Canadian Land Surface Scheme: model runs and sensitivity analysis at three boreal forest stands, Atmos. Ocean, 44, 207–222, 2006.

Brown, R., Bartlett, P., Mackay, M., and Verseghy, D.: Estimation of snow cover in CLASS for SnowMIP, Atmos. Ocean, 44, 223–238, 2006.

Christian, J. R., Arora, V. K., Boer, G. J., Curry, C. L., Zahariev, K., Denman, K. L., Flato, G. M., Lee, W. G., Merryfield, W. J., Roulet, N. T., and Scinocca, J. F.: The global carbon cycle in the Canadian Earth system model (CanESM1): Preindustrial control simulation, J. Geophys. Res., 115, G03014, doi:10.1029/2008JG000920, 2010.

Ciais, P., Sabine, C., Bala, G., Bopp, L., Brovkin, V., Canadell, J., Chhabra, A., DeFries, R., Galloway, J., Heimann, M., Jones, C., Le Quéré, C., Myneni, R. B., Piao, S., and Thornton, P.: Carbon and Other Biogeochemical Cycles, in: Climate Change 2013: The Physical Science Basis. Contribution of Working Group I to the Fifth Assessment Report of the Intergovernmental Panel on Climate Change, edited by: Stocker, T. F., Qin, D., Plattner, G.-K., Tignor, M., Allen, S. K., Boschung, J., Nauels, A., Xia, Y., Bex, V., and Midgley, P. M., Cambridge University Press, Cambridge, United Kingdom and New York, NY, USA, 2013.

da Rocha, H. R., Goulden, M. L., Miller, S. D., Menton, M. C., Pinto, L. D. V. O., De Freitas, H. C., and Silva Figueira, A. M. E.: Seasonality of water and heat fluxes over a tropical forest in eastern Amazonia, Ecol. Appl., 14, S22–S32, 2004.

Friedlingstein, P., Cox, P., Betts, R., Bopp, L., von Bloh, W., Brovkin, V., Cadule, P., Doney, S., Eby, M., Fung, I., Bala, G., John, J., Jones, C., Joos, F., Kato, T., Kawamiya, M., Knorr, W., Lindsay, K., Matthews, H. D., Raddatz, T., Rayner, P., Reick, C., Roeckner, E., Schnitzler, K.-G., Schnur, R., Strassmann, K., Weaver, A. J., Yoshikawa, C., and Zeng, N.: Climate–carbon cycle feedback analysis: Results from the C4MIP model intercomparison, J. Climate, 19, 3337–3353, 2006.

Garnaud, C., Sushama, L., and Arora, V. K.: The effect of driving climate data on the simulated terrestrial carbon pools and fluxes over North America, Int. J. Climatol., 34, 1098–1110, 2014.

Gillett, N. P., Arora, V. K., Matthews, D., and Allen, M. R.: Constraining the Ratio of Global Warming to Cumulative CO_2 Emissions Using CMIP5 Simulations, J. Climate, 26, 6844–6858, 2013.

Gourdji, S. M., Mueller, K. L., Yadav, V., Huntzinger, D. N., Andrews, A. E., Trudeau, M., Petron, G., Nehrkorn, T., Eluszkiewicz, J., Henderson, J., Wen, D., Lin, J., Fischer, M., Sweeney, C., and Michalak, A. M.: North American CO_2 exchange: inter-comparison of modeled estimates with results from a fine-scale atmospheric inversion, Biogeosciences, 9, 457–475, doi:10.5194/bg-9-457-2012, 2012.

Hoffman, F. M., Randerson, J. T., Arora, V. K., Bao, Q., Cadule, P., Ji, D., Jones, C. D., Kawamiya, M., Khatiwala, S., Lindsay, K., Obata, A., Shevliakova, E., Six, K. D., Tjiputra, J. F., Volodin, E. M., and Wu, T.: Causes and implications of persistent atmospheric carbondioxide biases in Earth System Models, J. Geophys. Res.-Biogeo., 119, 141–162, doi:10.1002/2013JG002381, 2014.

Houghton, R. A.: Carbon Flux to the Atmosphere from Land-Use Changes: 1850–2005, in: TRENDS: A Compendium of Data on Global Change, Carbon Dioxide Information Analysis Center, Oak Ridge National Laboratory, US Department of Energy, Oak Ridge, Tenn., USA, 2008.

Hurtt, G. C., Chini, L. P., Frolking, S., Betts, R. A., Feddema, J., Fischer, G., Fisk, J. P., Hibbard, K., Houghton, R. A., Janetos, A., Jones, C. D., Kindermann, G., Kinoshita, T., Klein Goldewijk, K., Riahi, K., Shevliakova, E., Smith, S., Stehfest, E., Thomson, A., Thornton, P., van Vuuren, D. P., and Wang, Y. P.: Harmo-

nization of land-use scenarios for the period 1500–2100: 600 years of global gridded annual land-use transitions, wood harvest, and resulting secondary lands, Climatic Change, 109, 117–161, doi:10.1007/s10584-011-0153-2, 2011.

Jones, C., Robertson, E., Arora, V., Friedlingstein, P., Shevliakova, E., Bopp, L., Brovkin, V., Hajima, T., Kato, E., Kawamiya, M., Liddicoat, S., Lindsay, K., Reick, C. H., Roelandt, C., Segschneider, J., and Tjiputra, J.: Twenty-First-Century Compatible CO_2 Emissions and Airborne Fraction Simulated by CMIP5 Earth System Models under Four Representative Concentration Pathways, J. Climate, 26, 4398–4413, 2013.

Keeling, C. D., Chin, J. F. S., and Whorf, T. P.: Increased activity of northern vegetation inferred from atmospheric CO_2 measurements, Nature, 382, 146–149, 1996.

Khatiwala, S., Primeau, F., and Hall, T.: Reconstruction of the history of anthropogenic CO_2 concentrations in the ocean, Nature, 462, 346–349, 2009.

Knol, M. J., Pestman, W. R., and Grobbee,D. E.: The (mis)use of overlap of confidence intervals to assess effect modification, Eur. J. Epidemiol., 26, 253–254, 2011.

Knorr, W.: Is the airborne fraction of anthropogenic CO_2 emissions increasing?, Geophys. Res. Lett., 36, L21710, doi:10.1029/2009GL040613, 2009.

Le Quéré, C., Moriarty, R., Andrew, R. M., Peters, G. P., Ciais, P., Friedlingstein, P., Jones, S. D., Sitch, S., Tans, P., Arneth, A., Boden, T. A., Bopp, L., Bozec, Y., Canadell, J. G., Chini, L. P., Chevallier, F., Cosca, C. E., Harris, I., Hoppema, M., Houghton, R. A., House, J. I., Jain, A. K., Johannessen, T., Kato, E., Keeling, R. F., Kitidis, V., Klein Goldewijk, K., Koven, C., Landa, C. S., Landschützer, P., Lenton, A., Lima, I. D., Marland, G., Mathis, J. T., Metzl, N., Nojiri, Y., Olsen, A., Ono, T., Peng, S., Peters, W., Pfeil, B., Poulter, B., Raupach, M. R., Regnier, P., Rödenbeck, C., Saito, S., Salisbury, J. E., Schuster, U., Schwinger, J., Séférian, R., Segschneider, J., Steinhoff, T., Stocker, B. D., Sutton, A. J., Takahashi, T., Tilbrook, B., van der Werf, G. R., Viovy, N., Wang, Y.-P., Wanninkhof, R., Wiltshire, A., and Zeng, N.: Global carbon budget 2014, Earth Syst. Sci. Data, 7, 47–85, doi:10.5194/essd-7-47-2015, 2015.

Ma, X., von Salzen, K., and Li, J.: Modelling sea salt aerosol and its direct and indirect effects on climate, Atmos. Chem. Phys., 8, 1311–1327, doi:10.5194/acp-8-1311-2008, 2008.

McGuire, A. D., Melilli, J. M., and Joyce, L. A.: The role of nitrogen in the response of forest net primary productivity to elevated atmospheric carbon dioxide, Annual Reviews of Ecology and Systematics, 26, 473–503, 1995.

Medlyn, B. E., Badeck, F.-W., De Pury, D. G. G., Barton, C. V. M., Broadmeadow, M., Ceulemans, R., De Angelis, P., Forstreuter, M., Jach, M. E., Kellomäki, S., Laitat, E., Marek, M., Philippot, S., Rey, A., Strassemeyer, J., Laitinen, K., Liozon, R., Portier, B., Roberntz, P., Wang, K., and Jstbid, P. G.: Effects of elevated [CO2] on photosynthesis in European forest species: a meta-analysis of model parameters, Plant Cell Environ., 22, 1475–1495, 1999.

Melton, J. R. and Arora, V. K.: Sub-grid scale representation of vegetation in global land surface schemes: implications for estimation of the terrestrial carbon sink, Biogeosciences, 11, 1021–1036, doi:10.5194/bg-11-1021-2014, 2014.

Melton, J. R., Shrestha, R. K., and Arora, V. K.: The influence of soils on heterotrophic respiration exerts a strong control on net ecosystem productivity in seasonally dry Amazonian forests, Biogeosciences, 12, 1151–1168, doi:10.5194/bg-12-1151-2015, 2015.

Namazi, M., von Salzen, K., and Cole, J. N. S.: Simulation of black carbon in snow and its climate impact in the Canadian Global Climate Model, Atmos. Chem. Phys., 15, 10887–10904, doi:10.5194/acp-15-10887-2015, 2015.

Peng, Y., von Salzen, K., and Li, J.: Simulation of mineral dust aerosol with Piecewise Log-normal Approximation (PLA) in CanAM4-PAM, Atmos. Chem. Phys., 12, 6891–6914, doi:10.5194/acp-12-6891-2012, 2012.

Peng, Y., Arora, V. K., Kurz, W. A., Hember, R. A., Hawkins, B. J., Fyfe, J. C., and Werner, A. T.: Climate and atmospheric drivers of historical terrestrial carbon uptake in the province of British Columbia, Canada, Biogeosciences, 11, 635–649, doi:10.5194/bg-11-635-2014, 2014.

Phillips, O. L. and Lewis, S. L.: Evaluating the tropical forest carbon sink, Glob. Change Biol., 20, 2039–2041, doi:10.1111/gcb.12423, 2014.

Pongratz, J., Reick, C. H., Houghton, R. A., and House, J. I.: Terminology as a key uncertainty in net land use and land cover change carbon flux estimates, Earth Syst. Dynam., 5, 177–195, doi:10.5194/esd-5-177-2014, 2014.

Ramankutty, N., Gibbs, H. K., Archard, F., DeFries, R., Foley, J. A., and Houghton, R. A.: Challenges to estimating carbon emissions from tropical deforestation, Glob. Change Biol., 13, 51–66, 2007.

Randerson, J. T., Thompson, M. V., Conway, T. J., Fung, I. Y., and Field, C. B.: The contribution of terrestrial sources and sinks to trends in the seasonal cycle of atmospheric carbon dioxide, Global Biogeochem. Cy., 11, 535–560, 1997.

Schimel, D., Stephens, B. B., and Fisher, J. B.: Effect of increasing CO_2 on the terrestrial carbon cycle, P. Natl. Acad. Sci. USA, 112, 436–441, doi:10.1073/pnas.1407302112, 2015.

Sturm, M., Holmgren, J., König, M., and Morris, K.: The thermal conductivity of seasonal snow, J. Glaciol., 43, 26–41, 1997.

Tabler, R. D., Benson, C. S., Santana, B. W., and Ganguly, P.: Estimating snow transport from 30 wind speed records: estimates versus measurements at Prudhoe Bay, Alaska, in: Proc. 58th Western Snow Conf., Sacramento, CA, 61–78, 1990.

Taylor, K. E., Stouffer, R. J., and Meehl, G. A.: An Overview of CMIP5 and the Experiment Design, B. Am. Meteorol. Soc., 93, 485–498, 2012.

Verseghy, D. L.: CLASS-the Canadian land surface scheme (version 3.6) – technical documentation. Internal report, Climate Research Division, Science and Technology Branch, Environment Canada (Downsview, Toronto, Ontario), 2012.

von Salzen, K.: Piecewise log-normal approximation of size distributions for aerosol modelling, Atmos. Chem. Phys., 6, 1351–1372, doi:10.5194/acp-6-1351-2006, 2006.

von Salzen, K., Scinocca, J. F., McFarlane, N. A., Li, J., Cole, J. N. S., Plummer, D., Verseghy, D., Reader, M. C., Ma, X., Lazare, M., and Solheim, L.: The Canadian fourth generation atmospheric global climate model (CanAM4). Part I: Representation of physical processes, Atmos. Ocean, 51, 104–125, doi:10.1080/07055900.2012.75561, 2013.

Wei, X., Shao, M., Gale, W., and Li, L.: Global pattern of soil carbon losses due to the conversion of forests to agricultural land, Scientific Reports, 4, 4062, doi:10.1038/srep04062, 2014.

Zaehle, S., Medlyn, B. E., De Kauwe, M. G., Walker, A. P., Dietze, M. C., Hickler, T., Luo, Y., Wang, Y.-P., El-Masri, B., Thornton, P., Jain, A., Wang, S., Warlind, D., Weng, E., Parton, W., Iversen, C. M., Gallet-Budynek, A., McCarthy, H., Finzi, A., Hanson, P. J., Prentice, I. C., Oren, R., and Norby, R.: Evaluation of 11 terrestrial carbon–nitrogen cycle models against observations from two temperate Free-Air CO_2 Enrichment studies, New Phytol., 202, 803–822, doi:10.1111/nph.12697, 2014.

Zeng, N., Zhao, F., Collatz, G. J., Kalnay, E., Salawitch, R. J., West, T. O., and Guanter, L.: Agricultural Green Revolution as a driver of increasing atmospheric CO_2 seasonal amplitude, Nature, 515, 394–397, 2014.

Zobler, L.: A World Soil File for Global Climate Modelling, NASA Technical Memorandum 87802, NASA Goddard Institute for Space Studies, New York, New York, USA, 1986.